

Active Brownian Heat Engines

Viktor Holubec,^{1,2,*} Stefano Steffenoni,^{1,3} Gianmaria Falasco,^{1,4} and Klaus Kroy¹

¹*Institut für Theoretische Physik, Universität Leipzig, Postfach 100 920, D-04009 Leipzig, Germany*

²*Charles University, Faculty of Mathematics and Physics, Department of*

Macromolecular Physics, V Holešovičkách 2, CZ-180 00 Praha, Czech Republic

³*Max Planck Institute for Mathematics in the Sciences, Inselstr. 22, D-04103 Leipzig, Germany*

⁴*Complex Systems and Statistical Mechanics, Department of Physics and
Materials Science, University of Luxembourg, L-1511 Luxembourg, Luxembourg*

(Dated: April 21, 2022)

We investigate active Brownian heat engines consisting of a Brownian particle confined in a modulated harmonic potential and immersed in a non-equilibrium bath of variable activity. We show that their average energetics determined by the second moment of the particle position can be mapped onto that of a model with a passive equilibrium bath at a suitably defined time-dependent effective temperature. Formal limitations for the thermodynamic performance, including maximum efficiency, efficiency at maximum power, and maximum efficiency at fixed power ensue. They help to clarify the degree to which such active heat engines can outperform passive-bath designs, which has been a debated issue for recent experimental realizations. And they can guide the design of new micro-machines. To illustrate the general principles, we analyze a specific realization of an active heat engine based on the paradigmatic Active Brownian Particle (ABP) model. Explicit analytical and numerical results are provided and discussed for quasi-static and finite-rate protocols. They reveal some non-intuitive features of the dynamical effective temperature, which complicate the implementation of classical cycles (like Carnot or Stirling) with active baths, illustrate various conceptual and practical limitations of the effective-equilibrium mapping, and clarify the operational relevance of various coarse-grained measures of dissipation.

PACS numbers: 05.20.-y, 05.70.Ln

I. INTRODUCTION

The study of heat engines is as old as the industrialization of the world. Its practical importance has prompted physicists and engineers to persistently improve their experiments and theories to eventually establish the consistent theoretical framework of classical thermodynamics. It allows to quantify, on a phenomenological level, how work is transformed to heat, and to what extent this process can be reversed. Heat is the most abundant form of energy, namely “disordered” energy dispersed among microscopic degrees of freedom, and turning it into the macroscopically coherent form called work has been a central aim since the days of Carnot, Stirling, and other pioneers, after whom some common designs have been named.

Recent advances in technology have allowed and also required to extend this success story into two new major directions. First, towards microscopic designs that are so small that their operation becomes stochastic rather than deterministic [1–4]. And secondly to cases where the degrees of freedom of the heat bath are themselves driven far from equilibrium, which potentially matters for small systems operating in a biological context, e.g., inside living cells or bacterial colonies [5].

The analysis of small systems requires an extension of the theory and basic notions of classical thermodynam-

ics to stochastic dynamics, which goes under the name of stochastic thermodynamics [6–9]. It seeks to define heat, work, and entropy on the level of individual stochastic trajectories. While the resulting average thermodynamics recovers the 2nd law, the theory allows to additionally quantify the probability of rare large fluctuations [9]. Many recent studies have been devoted to realizations of microscopic thermodynamic cycles. See, for example, Refs. [10–15] for experimental studies and Refs. [16–25] for theoretical ones. In this field, Brownian heat engines play a paradigmatic role [13–15, 24, 25]. They are based on a colloidal particle representing the working substance. It diffuses in an equilibrium bath but is confined by a time-dependent potential, realizable in practice by optical tweezers, in place of a volume-regulating piston [13, 14, 26].

The following discussion concerns an idealized minimal model of such Brownian heat engines, but combines it with the mentioned second recent extension of the classical field of heat engines. Namely, over the last few years, increasing effort has been devoted to study the thermodynamics of quantum [27, 28] and classical (colloidal) [5, 29–31] heat engines that operate in contact with a non-equilibrium “active” bath. Paradigmatic realizations of such active baths are, for example, suspensions of self-propelling bacteria or synthetic microswimmers [5, 32]. They are driven far from equilibrium on the level of the individual particles and not merely by externally imposed overall boundary or body forces. The corresponding “active heat engines” can outperform classical designs. The main trick is to evade the zeroth law of thermodynamics

* viktor.holubec@mff.cuni.cz

by operating very far from equilibrium, so that various degrees of freedom do not mutually thermalize. Exploiting this unconventional property, these engines can operate between hugely different (effective) temperatures and thereby at unconventionally high efficiencies — without risking the evaporation or freezing of the laboratory. Active heat engines have moreover been claimed to transcend the universal performance bounds set by the second law of thermodynamics [5], a notion that is critically examined below. To elucidate our general results and conclusions by a specific model, we provide a detailed analysis of a special active Brownian heat engine. Its design is based on the standard minimal model for active particle suspensions, namely the so-called ABP (“active Brownian particle”) model [33], which is why we want to refer to it by the reminiscent acronym ABE (“active Brownian engine”), in the following. The possibility to perform explicit analytical and numerical computations allow the potential merits and limitations of active heat engines to be analyzed and illustrated quantitatively and in considerable detail.

II. SETUP AND MAIN RESULTS

In all of the following, we consider a heat engine consisting of a particle confined to a *time-dependent harmonic* potential

$$V(x, y, t) = \frac{1}{2}k(t)\mathbf{r}^2 = \frac{1}{2}k(t)(x^2 + y^2), \quad (1)$$

with an externally controlled stiffness $k(t)$, and immersed in a (possibly) non-equilibrium bath, described by a zero-mean *additive* noise $\boldsymbol{\eta}(t)$. We assume that the dynamics of the particle position $\mathbf{r} = (x, y)^\top$ obeys the *overdamped linear* Langevin equation

$$\dot{\mathbf{r}} = -\mu k(t)\mathbf{r}(t) + \boldsymbol{\eta}(t). \quad (2)$$

Depending on the noise correlations, which remain to be prescribed and need not be Markovian, and depending on the physical interpretation, this model can describe various experimentally relevant situations. In Fig. 1 we depict two of them that we discuss further below: namely, an active particle or “microswimmer” immersed in a passive equilibrium bath (left) [34, 35], and a (passive) colloid immersed in an active non-equilibrium bath that is itself composed of active particles swimming in a thermal background solvent (right) [36–40]. Further examples are provided by devices that share the same formal description on a suitably coarse-grained level, such as noisy electric circuits and similar Langevin systems [41].

In line with such realizations, the trapping potential (1) has the harmonic standard form experimentally created with the help of optical tweezers [5, 13, 14]. We have also taken advantage of the fact that such experiments are typically designed in a quasi two-dimensional geometry, in narrow gaps between two glass coverslips.

For simplicity, the particle mobility is represented by a constant scalar μ and the two-time correlation matrix $C_{ij}(t, t') \equiv \langle \eta_i(t)\eta_j(t') \rangle \propto \delta_{ij}$ of the noise $\boldsymbol{\eta} = (\eta_x, \eta_y)$ by a diagonal form. Our analysis can of course straightforwardly be generalized to arbitrary dimensions and mobility matrices. Also, with the formalism of Ref. [42, 43], one could extend it to linear memory kernels to represent underdamped or otherwise correlated dynamics.

If $\boldsymbol{\eta}$ in Eq. (2) stands for the white noise, the model provides a good description for existing experimental realisations of Brownian heat engines [14, 44]. Their thermodynamics has been thoroughly analyzed in the literature [24, 45, 46]. An example for an experimental realisation of the non-equilibrium-noise version is the active Brownian engine with a bacterial bath, studied by Krishnamurthy et al. [5]. The performance of a quasi-static Stirling heat engine based on the latter design was already nicely analyzed by Zakine et al. [29]. Its finite-time performance was numerically investigated in Ref. [31]. With respect to these studies, which employ specific protocols, our approach is valid for arbitrary driving protocols at arbitrary speeds.

As a main result, we show in the following that the thermodynamics of the system described by Eq. (2) with a non-equilibrium noise $\boldsymbol{\eta}$, to which we refer as the *active* model, can be mapped onto the well-investigated model with a passive equilibrium bath [24, 45, 46], to which we refer as the *passive/equilibrium* model:

$$\dot{\mathbf{r}}(t) = -\mu k(t)\mathbf{r}(t) + \sqrt{2D_{\text{eff}}(t)}\boldsymbol{\xi}(t). \quad (3)$$

Its bath is characterized by the Gaussian white noise $\boldsymbol{\xi}(t)$ with zero mean, $\langle \boldsymbol{\xi}(t) \rangle = 0$, the unit correlation matrix $\langle \xi_i(t)\xi_j(t') \rangle = \delta_{ij}\delta(t-t')$, and a time-dependent (effective) temperature [47]

$$T_{\text{eff}}(t) = \frac{D_{\text{eff}}(t)}{k_B\mu} = \frac{1}{2\mu} \langle \mathbf{r}(t) \cdot \boldsymbol{\eta}(t) \rangle. \quad (4)$$

Below, the latter is shown to follow solely from the two-time correlation matrix $C(t, t')$ of the noise $\boldsymbol{\eta} = (\eta_x, \eta_y)$. Since the passive model (3) and the corresponding temperature (4) describe the active model only effectively, in terms of its average thermodynamic properties, (3) and (4) are referred to as an effective passive/equilibrium model and an effective temperature, respectively.

The existence of this mapping immediately implies that the performance of the active heat engine in terms of its output power and efficiency is precisely that of the corresponding effective equilibrium model. Therefore, the known bounds on (finite-time) performance of cyclic Brownian heat engines described by Eq. (3), such as the ultimate Carnot efficiency bound [48], the efficiency at maximum power [24], the maximum efficiency at arbitrary power [45, 49], and the possibility to almost attain the reversible efficiency at nonzero power [46], directly carry over to the active heat engine. Furthermore, the effective equilibrium model also sets bounds on average thermodynamic variables for non-cyclic and even transient processes. Yet, the non-equilibrium character of the

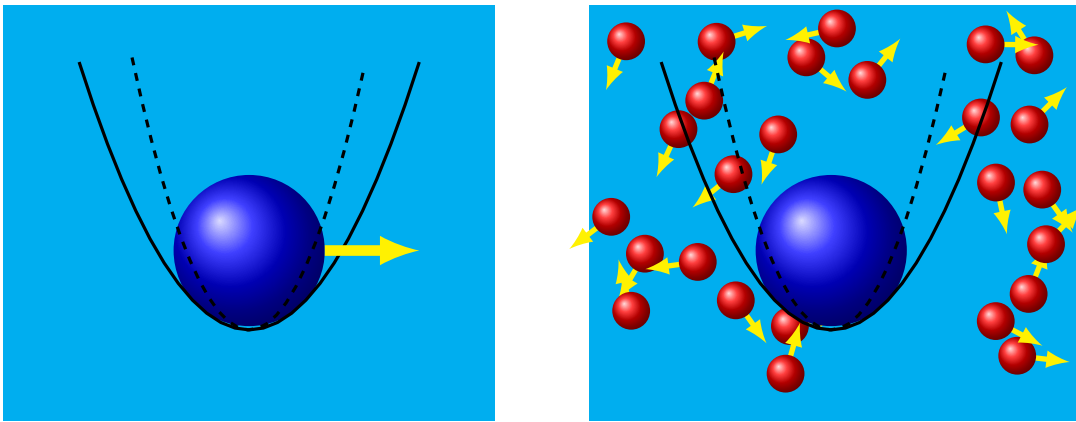


FIG. 1. Schematic designs of microscopic heat engines based on colloids in modulated harmonic traps, playing the roles of the working substance and the movable piston, respectively. Left: active particle in a “passive” equilibrium bath. Right: passive particle in an “active” non-equilibrium bath composed of energy consuming micro-swimmers immersed into a passive background fluid. To operate the heat engine, the bath temperature and/or activity and the confinement strength are modulated cyclically. Thereby “disordered” energy dispersed in the bath and randomly propelling the colloid against its confinement is concentrated in a degree of freedom that can be externally harnessed to perform (mechanical) work.

underlying dynamics reveals itself upon closer inspection, as detailed in the remainder of the paper.

III. OUTLINE OF THE PAPER

The paper is organized as follows. In the next Sec. IV, we define the thermodynamic variables describing the performance of the heat engine. In Section V, the effective temperature (4) is derived and the equivalence of the active and effective passive models, (2) and (3), is proven, which are our main results.

The following Sec. VI describes consequences of the mapping to equilibrium. Specifically, Sec. VIA contains a detailed description of the passive model, and Sec. VIB reviews its thermodynamic behavior both for quasi-static and finite-time cyclic driving. In Sec. VIC, we discuss a recent experimental realization of an active heat engine with a bacterial bath in the light of our results, and clarify the status of the reported extraordinary efficiency values.

Readers familiar with the concept of effective temperature and the standard stochastic thermodynamics of colloidal heat engines may want to skip (parts of) this section and continue directly with Sec. VII, where we exemplify our results by a worked example based on the paradigmatic active Brownian particle (ABP) model, to which we refer to as to ABE. The following Sec. VIII introduces alternative interpretations of the ABP model and the corresponding dissimilar contributions to the entropy production that denounces the non-equilibrium character of the engine that persists during nominally reversibly operation. Readers familiar with this model may wish to jump to Sec. IX A, where we analyze the quasi-static performance of the ABE and some peculiarities of the effective bath temperature. The finite-time performance of the ABE is discussed in Sec. IX B. For

better readability, various details concerning the ABP dynamics, the definitions of the various entropies, and the positional distribution function have been deferred to an Appendix. We conclude in Sec. X.

For the remainder of the paper and in the figures, we set the Boltzmann constant to unity, $k_B = 1$, which amounts to measuring energies in Kelvin. The ubiquitous time argument t of the thermodynamic variables is occasionally tacitly omitted.

IV. THERMODYNAMIC VARIABLES

In standard macroscopic thermodynamics, quantities such as work and heat are functionals on system trajectories in the thermodynamic state-space. For small systems, described by *stochastic* differential equations and stochastic trajectories $\{\mathbf{r}(t)\}$, also work and heat become stochastic functionals. See for example Refs. [8, 9] for systems in contact with equilibrium baths and Ref. [50] for a system in contact with an active bath. Here, we are interested in noise-averaged values of these functionals, which can be constructed from the internal energy of the process (2), namely

$$U(t) = \langle V \rangle = \frac{1}{2}k(t) [\sigma_x(t) + \sigma_y(t)] = \frac{1}{2}k(t)\sigma(t), \quad (5)$$

where $\sigma_x = \langle x^2 \rangle$, $\sigma_y = \langle y^2 \rangle$, and $\sigma = \langle \mathbf{r} \cdot \mathbf{r} \rangle$. For periodic driving, the average state of the system eventually, after a transient period, attains a time-periodic steady state. And due to the symmetry of the potential, the average particle displacements $\langle x \rangle$ and $\langle y \rangle$ during the cycle will be zero, so that the mean square displacements $\sigma_x(t)$ and $\sigma_y(t)$ also determine the long-time variances for the x - and y -coordinates, respectively.

Combining Eq. (5) with the first law of thermodynamics, $\dot{U}(t) = \dot{W}(t) + \dot{Q}(t)$, we identify the work done on the particle during the time interval (t_i, t_f) ,

$$\begin{aligned} W(t_i, t_f) &= \int_{t_i}^{t_f} dt \dot{W}(t) \\ &= \frac{1}{2} \int_{t_i}^{t_f} dt \dot{k}(t) \sigma(t) = \frac{1}{2} \int_{k(t_i)}^{k(t_f)} dk \sigma, \end{aligned} \quad (6)$$

as the energy flowing into the system from an external source controlling the potential, and the heat,

$$\begin{aligned} Q(t_i, t_f) &= \int_{t_i}^{t_f} dt \dot{Q}(t) \\ &= \frac{1}{2} \int_{t_i}^{t_f} dt k(t) \dot{\sigma}(t) = \frac{1}{2} \int_{\sigma(t_i)}^{\sigma(t_f)} d\sigma k, \end{aligned} \quad (7)$$

as the energy flowing into the system from the reservoir.

The performance of an engine is most commonly quantified in terms of output power P and efficiency η . In the present case, these variables read

$$P \equiv \frac{W_{\text{out}}}{t_p}, \quad \eta \equiv \frac{W_{\text{out}}}{Q_{\text{in}}}. \quad (8)$$

Here, $W_{\text{out}} = -W(0, t_p)$ is the work done by the engine per cycle of duration t_p . We employ the unit step function $\Theta(x)$ to express the heat flowing from the bath into the system as

$$Q_{\text{in}} = \int_0^{t_p} dt \dot{Q}(t) \Theta[\dot{Q}(t)] \quad (9)$$

While the definition of the output power bares no controversy, it must be stressed that our definition of the efficiency neglects the energy required to maintain the non-equilibrium state of the bath, which is sometimes referred to as the housekeeping heat.

However, we argue that this is the correct way to assess the efficiency of engines in contact with non-equilibrium reservoirs. In analogy with standard heat engines, we treat energy exchanged with degrees of freedom under precise experimental control as work and energy exchanged with not explicitly resolved degrees of freedom as heat. For the situation depicted in Fig. 1, the degree of freedom under control is the particle position and the remaining degrees of freedom (particle orientation, state of the surrounding fluid, etc.) represent the bath. Importantly, this means that the boundary between work and heat depends on the skills of the experimentalist. Take as an example the active particle depicted in Fig. 1a). For an experimentalist controlling just the stiffness of the potential, the distinction between heat and work is as described above. In contrast, if the active particle could signal its future path, this additional information could be utilized to exploit its self-propulsion to perform useful work (without need for the potential). In such a

case, however, the definition of efficiency would have to be modified to acknowledge the house-keeping power required for the self-propulsion. It would thereby turn into a measure of efficiency for the work-to-work conversion in the noisy environment.

V. EFFECTIVE TEMPERATURE

A. General formulation

It is noteworthy that all of the above thermodynamic quantities are determined solely by the variance σ , which obeys the ordinary differential equation

$$\dot{\sigma}(t) = -2\mu k(t)\sigma(t) + 2 \langle \mathbf{r}(t) \cdot \boldsymbol{\eta}(t) \rangle. \quad (10)$$

The latter follows from Eq. (2) by taking the scalar products of \mathbf{r} and both sides and averaging over the noise. For arbitrary additive noise $\boldsymbol{\eta}$, Eq. (2) has the formal solution

$$\mathbf{r}(t) = \mathbf{r}_0 e^{-K(t, t_0)} + \int_{t_0}^t dt' \boldsymbol{\eta}(t') e^{-K(t, t')}, \quad (11)$$

with $K(t, t') \equiv \mu \int_{t'}^t dt'' k(t'')$ and $\mathbf{r}_0 \equiv \mathbf{r}(0)$ denoting an arbitrary initial position of the particle. Together with the two-time noise correlation matrix, $C(t, t')$, the average in Eq. (10) evaluates to

$$\begin{aligned} \langle \mathbf{r}(t) \cdot \boldsymbol{\eta}(t) \rangle &= 2D_{\text{eff}}(t) \equiv \langle \mathbf{r}_0 \cdot \boldsymbol{\eta}(t) \rangle e^{-K(t, t_0)} + \\ &2 \int_{t_0}^t dt' \text{Tr}[C(t, t')] e^{-K(t, t')}, \end{aligned} \quad (12)$$

where Tr denotes the trace operation. A crucial observation is that it therefore assumes a form that would also result from the Gaussian white noise $\boldsymbol{\eta} = \sqrt{2D_{\text{eff}}(t)} \boldsymbol{\xi}(t)$ with the correlation matrix $C_{ij}(t, t') = 2\sqrt{D_{\text{eff}}(t)D_{\text{eff}}(t')} \delta_{ij} \delta(t - t')$. This implies that the average thermodynamic behavior of the active model (2) with arbitrary additive noise is the same as that of the passive model (3) with an effective equilibrium bath temperature

$$T_{\text{eff}}(t) = \frac{D_{\text{eff}}(t)}{\mu} = \frac{1}{2\mu} \langle \mathbf{r}(t) \cdot \boldsymbol{\eta}(t) \rangle = \frac{k\sigma}{2} + \frac{\dot{\sigma}}{4\mu}. \quad (13)$$

The last expression follows from Eq. (10). It shows that also the effective temperature is uniquely given by the variance σ . Notably, the result (13) is valid arbitrarily far from equilibrium and it does not follow from any close-to-equilibrium linear-response approximation like in the Green-Kubo formula [51].

Also note that for positive effective temperature $T_{\text{eff}}(t) \geq 0$, Eq. (13) establishes the announced mapping between the active and passive heat engine and thus proves our main result. Negative effective temperatures can however be obtained, for example, during transients departing from initial conditions with $\langle \mathbf{r}_0 \cdot \boldsymbol{\eta}(t) \rangle < 0$. At

late times, the sign of the effective temperature is determined by the integral in Eq. (12), which is positive for standard correlation matrices $C(t, t')$ with non-negative diagonal elements. For a quasi-static process, where the system parameters vary slowly compared to the intrinsic relaxation times, one can neglect $\dot{\sigma}(t)$ relative to the other terms in Eq. (13). The effective temperature then reduces to the well-known form [5]

$$T_{\text{eff}}(t) = k(t)\sigma(t)/2. \quad (14)$$

For slowly driven systems, the effective temperature is thus always positive, thanks to the positivity of the trap stiffness k and variance σ .

B. Cyclic heat engines

The general definition (13) of the effective temperature applies both under transient and stationary conditions. Cyclic heat engines operate time-periodically by virtue of their periodic driving. Accordingly, we assume that the potential stiffness $k(t)$ is a periodic function with period t_p and that the noise correlation matrix is of the form

$$C_{ij}(t, t') = 2\delta_{ij}I(t)I(t')f_i(t - t'), \quad (15)$$

where $I(t)$ stands for a t_p -periodic intensity of the noise, and $f_i(t)$ are arbitrary functions obeying $f_i(0) = 1$ and decaying towards zero as $t \rightarrow \infty$. The system dynamics then settles onto a time-periodic attractor, independent of the initial condition \mathbf{r}_0 , at late times. From now on, we assume that the engine operates in this “steady state” regime, to which we refer as the *limit cycle*. During the cycle, the effective temperature $T_{\text{eff}}(t)$ takes the form [see Eqs. (12) and (13)]

$$\frac{1}{\mu}I(t) \int_{-\infty}^t dt' I(t')[f_x(t - t') + f_y(t - t')]e^{-K(t, t')}. \quad (16)$$

Importantly, for positive diagonal elements of the correlation matrix, the effective temperature is then manifestly positive, as required to map the active onto the passive model.

C. (Im)possible generalizations

The simplifying power of the present approach crucially relies on two main features. Firstly, on the linearity of Eq. (2), and secondly on the fact that thermodynamics is predominantly concerned with average energetics.

For the active heat engines discussed in the present contribution, the pertinent microscopic degree of freedom is the position of the colloid. Its thermodynamics is contained in the variance $\sigma = \langle \mathbf{r} \cdot \mathbf{r} \rangle$, which controls the complete average energetics (work and heat) of the engine through Eqs. (6) and (7). However, the described mapping to a passive-bath model cannot be extended beyond such average energetics, since the active (2) and

passive (19) models differ in variables which depend on higher moments of the position \mathbf{r} or its complete distribution. This is for example the case for the total entropy or the fluctuations of work, heat and entropy. Without further ado, one thus cannot take for granted the results obtained under the assumption of a perfect contact with an equilibrium bath, such as the Jarzynski equality [52], the Crooks fluctuation theorem [53], the Hatano-Sasa equality [54], and various inequalities containing higher moments of work, heat, and entropy, such as thermodynamic uncertainty relations [55–58].

Also note that, for a true equilibrium noise $\boldsymbol{\eta}$, the (effective) temperature T_{eff} in Eq. (4) would agree with all other possible definitions of temperature, thereby tying together many *a priori* unrelated dynamical quantities (e.g. by their structurally identical Boltzmann distributions or fluctuation-dissipation theorems, etc.). However, for a non-equilibrium noise, differently defined temperatures can (and generally will) have different values. We refer to Refs. [59–62] for various (complementary) approaches to effective temperatures and Refs. [63–65] for some reviews. Moreover, as illustrated by the ABP results (35)–(36) in App. D, typical non-equilibrium distributions deviate strongly from Boltzmann’s Gaussian equilibrium distribution, such as the one characterizing the long-time limit of the equilibrium process, Eq. (3), at constant T_{eff} — namely $\rho(\mathbf{r}) \propto \exp[-k\mathbf{r}^2/2T_{\text{eff}}]$. Therefore, in order to build an effective thermodynamic description from a non-equilibrium statistical-mechanics model, one generally has to calculate precisely the effective temperatures corresponding to the relevant degrees of freedom, under the prescribed conditions.

This leads to the mentioned second limitation of the presented effective-temperature mapping, namely that it hinges on the linearity of the model. To make the point, let us consider a one-dimensional setting with the potential $U(x, t) = k(t)x^n/n$ when the Langevin equation for position x reads

$$\dot{x}(t) = -k(t)[x(t)]^{n-1} + \eta(t) \quad (17)$$

and the internal energy, work, and heat (per unit time) are given by $U(t) = k(t) \langle [x(t)]^n \rangle$, $\dot{W}(t) = \dot{k}(t) \langle [x(t)]^n \rangle$, and, $\dot{Q}(t) = k(t)d \langle [x(t)]^n \rangle / dt$, respectively. In order to describe the average thermodynamics, we thus have to consider the dynamics of the n th moment $\langle [x(t)]^n \rangle$. Multiplying Eq. (17) by x^{n-1} and averaging the result over the noise, we find that

$$\frac{d}{dt} \langle [x(t)]^n \rangle = -nk(t) \langle [x(t)]^{2n-2} \rangle + n \langle [x(t)]^{n-1} \eta(t) \rangle. \quad (18)$$

Thus, in order to get an exact closed dynamical equation for $\langle [x(t)]^n \rangle$, we also need a dynamical equation for $\langle [x(t)]^{2n-2} \rangle$ which, in turn, depends on the moment $\langle [x(t)]^{3n-4} \rangle$, and so on. However, out of equilibrium each degree of freedom (and, also each moment $\langle [x(t)]^n \rangle$) has, in general, its own effective temperature, if such a set of effective temperatures can consistently be defined at all.

Recall that the development of a useful (finite-time) thermodynamic description based on a time-dependent effective temperature requires a system with equilibrium noise that yields the same (time-resolved) dynamics of the relevant moments, for which our above discussion of the variance of the linear model (2) provides the paradigm. This means that we would have to develop a passive model with an equilibrium noise that gives rise to precisely the same dynamics of all the moments in Eq. (18) as the original nonlinear active model. This can get very difficult if not impossible if the moments represent independent effective degrees of freedom so that their effective temperatures differ [66].

Despite these limitations, there are also many important properties that can successfully be captured by the effective-temperature mapping. In the next section, we review its general consequences for the performance of active heat engines. Readers familiar with stochastic thermodynamics may wish to continue directly with Sec. VII, where we derive and discuss more specific analytical results based on the so-called active Brownian particle (ABP) model with an exponential correlation matrix.

VI. EFFICIENCY

A. Effective entropy production

As described above, the dynamics of the variance in the active model (2) can be mimicked exactly by the effective passive model

$$\dot{\mathbf{r}}(t) = -\mu k(t)\mathbf{r}(t) + \sqrt{2D_{\text{eff}}(t)}\boldsymbol{\xi}(t) \quad (19)$$

with an equilibrium bath at the time-dependent temperature $T_{\text{eff}}(t)$, as long as the latter does not transiently turn negative. The noise intensity $D_{\text{eff}}(t)$ and the mobility $1/\mu$ in Eq. (19) are thus related by the fluctuation-dissipation relation $D_{\text{eff}} = \mu T_{\text{eff}}$. As discussed in Sec. IV, the variance determines the average thermodynamics of the active engine in terms of work, heat, and efficiency. In particular, due to our interpretation of thermodynamic variables above, the (average) performance of the active heat engine is the same as that of a passive heat engine based on Eq. (19) and can thus be taken over from the known thermodynamics of the passive model [8, 24, 25]. In fact, such a consistent thermodynamic framework is crucial for a meaningful concept of efficiency, far from equilibrium.

For pedagogical reasons and for completeness, we briefly review the thermodynamics of the effective passive model, here. The main result, to be derived below, is the explicit formulation of the second law of thermodynamics. It states that the active engine has a non-negative total effective entropy-production rate

$$\dot{S}_{\text{tot}}^{\text{eff}}(t) = \mu T_{\text{eff}}(t) \sigma(t) \left[\frac{2}{\sigma(t)} - \frac{k(t)}{T_{\text{eff}}(t)} \right]^2 \geq 0. \quad (20)$$

Thermodynamically, the entropy production can always be decomposed into the contributions

$$\dot{S}_{\text{tot}}^{\text{eff}}(t) = \dot{S}^{\text{eff}}(t) + \dot{S}_{\text{R}}^{\text{eff}}(t) \quad (21)$$

due to the working substance itself and due to the entropy change in the (effective) heat bath, respectively. Since, by definition, the heat flow from/into an equilibrium heat bath is reversible, the entropy change of the bath obeys the Clausius equality,

$$\dot{S}_{\text{R}}^{\text{eff}}(t) = -\frac{\dot{Q}(t)}{T_{\text{eff}}(t)} = -\frac{k(t)\dot{\sigma}(t)}{2T_{\text{eff}}(t)}, \quad (22)$$

where the last step exploits the definition (7) of the mutual heat-exchange rate $\dot{Q}(t)$. For the system entropy, one merely has the weaker Clausius inequality

$$\dot{S}^{\text{eff}}(t) \geq -dS_{\text{R}}^{\text{eff}}(t) = \dot{Q}(t)/T_{\text{eff}}(t). \quad (23)$$

It can be turned into an equality if a quasi-static driving protocol is employed, which then also optimizes the thermodynamic efficiency of the active heat engine.

We now show how these results follow from the statistical-mechanics description. First and foremost, note that the linearity of Eq. (19) ensures that the stochastic process $\mathbf{r}(t)$ is a linear functional of the Gaussian white noise $\boldsymbol{\xi}(t)$. The probability density for the particle position $\mathbf{r} = (x, y)$ at time t is therefore also Gaussian, namely

$$p^{\text{eff}}(x, y, t) = \frac{1}{\pi\sigma(t)} \exp\left[-\frac{(x^2 + y^2)}{\sigma(t)}\right], \quad (24)$$

and can easily be seen to solve the Fokker-Planck equation

$$\frac{\partial p^{\text{eff}}}{\partial t} = \nabla_{\mathbf{r}} \cdot [\mu \nabla_{\mathbf{r}} V(\mathbf{r}) + D_{\text{eff}} \nabla_{\mathbf{r}}] p^{\text{eff}} \quad (25)$$

with $\nabla_{\mathbf{r}} = (\partial_x, \partial_y)$. The corresponding Gibbs-Shannon entropy

$$\begin{aligned} S^{\text{eff}}(t) &= -\int_{-\infty}^{\infty} dx \int_{-\infty}^{\infty} dy p^{\text{eff}} \log p^{\text{eff}} \\ &= \log \sigma(t) + \log \pi + 1 \end{aligned} \quad (26)$$

is thus solely determined by the variance $\sigma(t)$ of the PDF (24), and therefore changes with the rate

$$\dot{S}^{\text{eff}}(t) = \frac{\dot{\sigma}(t)}{\sigma(t)}. \quad (27)$$

The second law in the form given in Eq. (20) now follows by inserting Eqs. (22) and (27) into Eq. (21) and using Eq. (10) for the time derivative of the variance in the form $\dot{\sigma} = 4\mu T_{\text{eff}}\sigma(1/\sigma - k/2T_{\text{eff}})$, after rearranging the resulting terms.

To make the entropy production vanish, which corresponds to the equal sign in Eqs. (20) and (23), one has to

drive the engine quasi-statically. This amounts to setting $\dot{\sigma} = 0$ in Eq. (13), which yields

$$\sigma(t) = \sigma_\infty(t) \equiv 2T_{\text{eff}}(t)/k(t). \quad (28)$$

For a quasi-static driving, the rates of change (22) and (27) of the reservoir and system entropies also both vanish, since they are proportional to the vanishing time derivative $\dot{\sigma} = 0$. However, this feature alone might not be enough for concluding that the entire entropy

$$\Delta S_{\text{tot}}^{\text{eff}}(t_p) = \int_0^{t_p} dt' \dot{S}_{\text{tot}}^{\text{eff}}(t') \quad (29)$$

throughout the whole cycle vanishes as $t_p \rightarrow \infty$, since it is sensitive to how large t_p has to be chosen to ensure quasi-static conditions, which depends on the intrinsic relaxation behavior of the working substance (in our case the trapped colloid) [67]. It is a consequence of the fluctuation dissipation relation fulfilled by the effective equilibrium model that the rates of change (22) and (27) of the reservoir and system entropies converge to each other fast enough that the whole quasi-static cycle is reversible, i.e. that (29) vanishes. We come back to this issue in Sec. VII, where we analyze an explicit model realization.

B. Efficiency bounds

For an arbitrary cycle, the Clausius inequality (23) can, via standard manipulations [68], be rewritten in terms of the quasi-static (qs) bounds for the output work W_{out} and efficiency η , respectively,

$$W_{\text{out}} \leq W_{\text{out}}^{\text{qs}}, \quad (30)$$

$$\eta \leq \eta^{\text{qs}} \leq \eta_C = 1 - \frac{\min(T_{\text{eff}})}{\max(T_{\text{eff}})}. \quad (31)$$

According to the discussion in the previous section, these conditions identically constrain the active heat engine. Given any driving protocol for the variation of the control parameters $k(t/t_p)$ and $T_{\text{eff}}(t/t_p)$, etc., along the cycle, the largest output work per cycle and the largest efficiency are thus attained for quasi-static driving with $t_p \rightarrow \infty$. The ultimate (Carnot) efficiency limit η_C for the active engine is thus reached in a quasi-static Carnot cycle composed of two ‘‘isothermal’’ branches, with constant T_{eff} , interconnected by two ‘‘adiabatic branches’’, with constant entropy (26) and variance σ_∞ .

Similarly, the mapping to the passive model (19) implies that the finite-time performance of the active heat engine is the same as that of its effective passive replacement. For convenience, we summarize some consequences of this observation, here. The quasi-static conditions, needed to reach the upper bound η_C on efficiency exactly, imply infinitely slow driving and thus vanishing output power. Naturally, such powerless heat engines are uninteresting for practical purposes [45], where only finite-time processes are relevant, and, thus, other measures of

engine performance have been proposed. A prominent role among them plays the maximum power condition. Schmiedl and Seifert [24] showed that overdamped Brownian heat engines deliver maximum power if they operate in the so called low-dissipation regime [69]. Their analysis implies that the efficiency at maximum power of the active heat engine is given by

$$\eta_{\text{MP}} = 1 - \sqrt{\frac{\min(T_{\text{eff}})}{\max(T_{\text{eff}})}}. \quad (32)$$

This result applies if the engine is driven along a finite-time Carnot cycle composed of two isotherms of constant T_{eff} and two infinitely fast adiabatic state changes at constant σ , with a suitable protocol for the trap stiffness $k(t)$ that minimizes the work dissipated during the isothermal branches. We also note that the maximum-power condition was investigated for a specific class of active colloidal heat engines in Ref. [30].

Actual technical realizations of heat engines are usually designed for a certain desired power output. Thus, even more useful than the knowledge of the efficiency at maximum power is the knowledge of maximum efficiency at a given power. Like the former, the latter is, for a Brownian heat engine of fixed design, attained when operating in the low-dissipation regime along a finite-time Carnot cycle [49, 70, 71]. The exact numerical and approximate analytical value of the maximum efficiency at arbitrary power for our setting can be obtained using the approach of Ref. [49]. Another universal result, applicable to the active Brownian heat engine, is that, for powers P close to the maximum power P^* , the efficiency increases infinitely fast with decreasing P (i.e. $|d\eta/dP|_{P \rightarrow P^*} \rightarrow \infty$) [49, 72]. Therefore, it is usually advantageous to operate heat engines close to maximum power conditions [small $\delta P = (P^* - P)/P^*$], rather than exactly at these conditions ($\delta P = 0$) [70]. Moreover, the results of Refs. [49, 70, 71] show that η_C can be attained only in the limit $\delta P \rightarrow 1$, where either the power P completely vanishes, or it is negligible with respect to the maximum power P^* . Recently, this insight led to a proposition of protocols yielding very large maximum power, thus allowing Brownian heat engines to operate close to (and practically with) Carnot’s efficiency at large output power [45, 46]. As discussed in the following paragraph, active Brownian heat engines offer an alternative route for achieving this.

C. Experiments

A relevant experimental realization of a system described by our model (2) is the bacterial heat engine of Ref. [5]. In this impressive experimental study, a colloidal particle trapped in a harmonic potential with a periodically modulated stiffness $k(t)$ was immersed in a bath of self-propelled bacteria with periodically modulated activity. The authors controlled the system parameters quasi-statically, along a Stirling cycle composed of

two isochoric state changes at constant trap stiffness k and two “isothermal” state changes at constant solvent temperature T and constant activity of the bacteria (in our notation corresponding to a constant strength T_{eff} of the noise $\boldsymbol{\eta}$). Driven by the periodic parameter modulation, the dynamics converged to a limit cycle, cyclically transforming energy absorbed from the disordered bacterial bath into a colloidal work. The authors measured the work done per cycle as well as the energy (heat) obtained per cycle from the bath and determined the efficiency of the machine as their ratio. They also measured the (quasi-static) effective temperature (14), which could be as high as 2000 K, suggesting that the engine could practically be operated at maximum efficiency.

We note, however, that the authors described their most surprising result as follows. “At high activities, the efficiency of our engines surpasses the equilibrium saturation limit of Stirling efficiency, the maximum efficiency of a Stirling engine where the ratio of cold to hot reservoir temperatures is vanishingly small.” This is indeed extraordinary, because it contradicts the limitations imposed by the effective passive model and the second law of thermodynamics, as described above. A possible explanation could be that the actual cycle does not correspond to the definition of a Stirling cycle [29]. For instance, a failure to control the pertinent effective temperature T_{eff} during the “isothermal” state changes could readily cause important deviations from the Stirling efficiency. However, Fig. 2a) of Ref. [5] strongly suggests that the effective temperature was actually carefully controlled during the state changes performed at constant bath temperature and bacterial activity, so that the actual effective cycle should indeed qualify as a proper Stirling cycle in the sense of our mapping to an effective passive bath.

This leaves us with an apparent paradox. The key to its resolution seems to lie in the definition of the efficiency employed in Ref. [5]. The authors measured the stochastic work output and heat input for individual cycles. The resulting mean values of work and heat were then obtained by averaging over several cycles, and the efficiency was formally expressed as their ratio. However, as can be inferred from Fig. 2 of Ref. [5], it was not actually evaluated according to this definition, but instead as the average of the work-over-heat ratio of individual cycles. The latter is not a well-behaved thermodynamic quantity, though [17, 73], since the distribution of the work-over-heat ratio per cycle is heavy-tailed and its moments do not exist. It therefore does not converge with increasing averaging time and can take more or less arbitrary values.

In summary, active heat engines can experimentally be operated very close to the optimum efficiency, which is universally delineated by the second law. The reason is that they allow extreme changes of the pertinent effective temperature to be realized with ordinary equipment, thanks to the breakdown of the zeroth law of thermodynamics for the non-equilibrium heat bath. Along the procedures outlined above, the appropriate consistent notion

of effective temperature for the active bath also follows from the second law.

In the following sections and in App. D, we explicitly analyze a specific realization of an active heat engine to illustrate the merits and limitations of the mapping to the passive model (19).

VII. WORKED EXAMPLE: THE ABE MODEL

A. Model definition

To exemplify the above findings for a specific model, we now consider the so-called ABP model. It is the standard minimal model for a particle embedded into an equilibrium bath at temperature T but actively propelling with velocity $\mathbf{v} = v\mathbf{n}(\theta)$ in the direction determined by the diffusing unit vector $\mathbf{n}(\theta)$ at angle $\theta(t)$. Encouraged by experimental evidence [5, 36, 37] and in accord with theoretical studies based on a rigorous elimination of (fast) active degrees of freedom [74, 75], the ABP model with harmonic confinement (Fig. 1a) has recently also been used to model passive Brownian colloids embedded in an active bath (Fig. 1b) [29, 31, 38–40]. Indeed, within the general formalism outlined above, the ABP model provides us with a simple realization of Eq. (2) in terms of a trapped colloid driven by the non-equilibrium noise

$$\boldsymbol{\eta} = \sqrt{2D(t)}\boldsymbol{\xi} + \mathbf{v}(t). \quad (33)$$

Here the components of $\boldsymbol{\xi} = (\xi_x, \xi_y)$ are mutually independent zero-mean unit-variance Gaussian white noises, but the velocity term $\mathbf{v} = v(t)\mathbf{n}(\theta)$ prohibits a straightforward equilibrium interpretation. It contributes an exponential term to the total noise correlation matrix

$$C_{ij}(t, t') = \langle \eta_i(t)\eta_j(t') \rangle = \delta_{ij} \left[2\sqrt{D(t)D(t')}\delta(t-t') + \frac{1}{2}v(t)v(t') \exp \left\{ - \int_{\min(t,t')}^{\max(t,t')} dt'' D_r(t'') \right\} \right]. \quad (34)$$

Such exponential memory has indeed also been found in a weak-coupling model for a passive tracer in an active bath [74, 76]. Besides, it is often employed as a tractable model for the complex correlations arising in strongly interacting systems. For the following, we assume that the translational diffusion coefficient $D(t)$ obeys the Einstein relation $D(t) = \mu T(t)$, but do not constrain the rotational diffusion coefficient $D_r(t)$ in the same way. The latter describes the free diffusion of the particle orientation $\mathbf{n} = \mathbf{v}/v$ on a unit circle and is incorporated into the ABP equations of motion [34, 77, 78] through yet another independent zero-mean unit-variance Gaussian white noise ξ_θ :

$$\dot{\mathbf{r}}(t) = -\mu k\mathbf{r}(t) + \mathbf{v}(t) + \sqrt{2D(t)}\boldsymbol{\xi}(t) \quad (35)$$

$$\dot{\theta}(t) = \sqrt{2D_r(t)}\xi_\theta(t). \quad (36)$$

That the ABP model provides a proper non-equilibrium active noise, as desired for Eq. (2), is not only apparent from the two-time correlation matrix (34), which fixes the average thermodynamics of the model in a way that is not consistent with a fluctuation-dissipation relation. It is further manifest in higher order correlation functions [79] that are sensitive to the non-Gaussian character of the noise (33). As illustrated in App. D, this for example allows for a bimodal distribution of the coordinates x and y , so that the ABP model captures some of the generically non-Gaussian character of non-equilibrium fluctuations, lost in another widely employed active-particle model that represents the active velocity as an Ornstein-Uhlenbeck process [35]. We note that these properties are essentially caused by the variable rotational noise ξ_θ and persist in a constant-speed ($v = \text{const.} \neq 0$) version of the model.

To emphasize the paradigmatic character of the heat engine described by the ABP-Eqs. (35)–(36) with periodically driven parameters $k(t)$, $T(t)$, $v(t)$, $D_r(t)$, we refer to it as the ABE model. It involves three ingredients that can potentially drive it far from equilibrium: (i) If the stiffness $k(t)$ changes on time-scales shorter than the intrinsic relaxation time, the particle dynamics is not fast enough to follow the protocol adiabatically. (ii) If the rotational diffusion coefficient D_r is not constrained by the Einstein relation, the rotational degree of freedom can be considered connected to a second bath at a temperature distinct from T . In general, connecting a system to several reservoirs at different temperatures drives it out of equilibrium. (iii) Finally, the velocity term in the Langevin system is formally identical to a non-conservative force giving rise to persistent currents that prevent equilibration.

B. Cyclic driving protocol

Our driving protocol involves a periodically modulated stiffness k , reservoir temperature T , rotational diffusion coefficient D_r , and active velocity v . We let the system evolve towards the limit cycle, where we analyze its performance. While the following theoretical discussion applies to arbitrary periodic driving, we exemplify our results with a specific Stirling-type protocol that mimics the experimental setup of Ref. [5] (see Fig. 2). It consists of four steps of equal duration ($t_p/4$):

(i) “Isothermal” compression A \rightarrow B: the stiffness k increases linearly from $k_<$ to $k_>$ at constant noise strength corresponding to the temperature $T = T_<$ and activity $\{D_r, v\} = \{D_r^<, v_<\}$.

(ii) “Isochoric” heating B \rightarrow C: the noise strength $\{T, D_r, v\}$ increases linearly from $\{T_<, D_r^<, v_<\}$ to $\{T_>, D_r^>, v_>\}$ at constant stiffness $k = k_>$.

(iii) “Isothermal” expansion C \rightarrow D: the stiffness decreases linearly from $k_>$ to $k_<$ at constant noise strength $\{T_>, D_r^>, v_>\}$.

(iv) “Isochoric” cooling D \rightarrow A: the noise strength

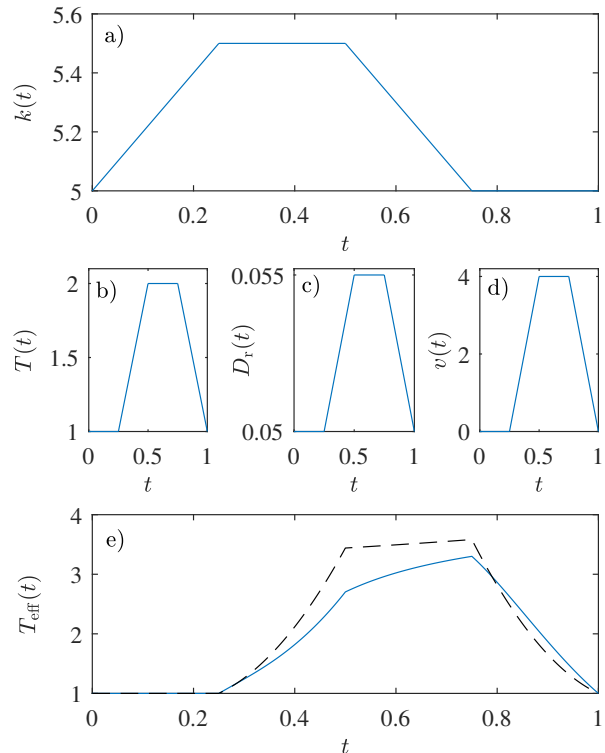


FIG. 2. The driving protocol of the ABE (a-d) and the effective temperature (e) that maps it to a passive model: a) trap stiffness, b) bath temperature, c) rotational diffusion coefficient, and d) active velocity, all as functions of time during the limit cycle. The full blue line in panel e) depicts the effective temperature $T_{\text{eff}}(t)$ of Eq. (44), the dashed line its limit (45) for a quasi-static (infinitely slow) driving. Parameters used: $t_p = 1$, $k_< = 5$, $k_> = 5.5$, $T_> = 2$, $T_< = 1$, $D_r^> = 0.055$, $D_r^< = 0.05$, $v_> = 4$, $v_< = 0$ and $\mu = 1$.

decreases back to its initial value at constant stiffness $k = k_<$.

Note that the “isothermal” state changes are characterized by constant bath temperature and activity, which in general corresponds to a varying effective temperature [see Fig. 2e)]. As explained in Sec. IV, the engine consumes (performs) work from A \rightarrow B (C \rightarrow D) while heat is absorbed (emitted) from (to) the reservoir from B \rightarrow C (D \rightarrow A).

C. Variance dynamics on the limit cycle

During the limit cycle, which is attained at late times, the dynamics of the variance $\sigma(t) = 2\sigma_x(t) = 2\sigma_y(t)$ [due to the symmetry of Eq. (35)] is for arbitrary time-periodic driving governed by the two coupled ordinary differential

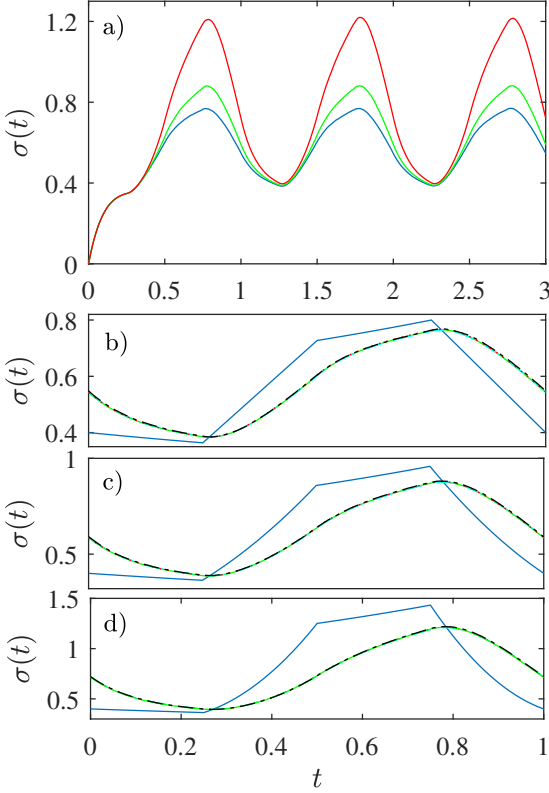


FIG. 3. Positional variance $\sigma(t) = \langle \mathbf{r} \cdot \mathbf{r} \rangle$ over time for the protocol shown in Fig. 2. Increasing activity $v_{>} = 0, 2, 4$ yields an increasing variance σ . a) BD simulations of the relaxation to the limit cycle. b) c) d) The dynamics on the limit cycle in BD simulations (solid green), numerical solutions [80] (dot-dashed black), and from the analytical formula (40) (dotted red), shows perfect agreement, despite considerable distance from the quasi-static limit (43) (broken blue lines).

equations

$$\dot{H}(t) = -[\mu k(t) + D_r(t)]H(t) + v(t), \quad (37)$$

$$\dot{\sigma}(t) = -2\mu k(t)\sigma(t) + 4D(t) + 2v(t)H(t). \quad (38)$$

Here, the term $2D(t) + v(t)H(t)$ determines the long-time time-periodic behavior of the average $\langle \mathbf{r}(t) \cdot \boldsymbol{\eta}(t) \rangle$. See App. A for details and for the derivation of the time-periodic solution

$$H = H_0 e^{-K(t,0) - F(t,0)} + \int_0^t v(s) e^{-K(t,s) - F(t,s)}, \quad (39)$$

$$\sigma = \sigma_0 e^{-2K(t,0)} + 4 \int_0^t dt' D_{\text{eff}}(t') e^{-2K(t,t')} \quad (40)$$

with functions $K(t, t_0) = \mu \int_{t_0}^t dt' k(t')$, $F(t, t_0) = \int_{t_0}^t dt' D_r(t')$, and $D_{\text{eff}}(t) = D(t) + v(t)H(t)/2$. The con-

stants

$$H_0 = \frac{\int_0^{t_p} dt' v(t') e^{-K(t_p, t') - F(t_p, t')}}{1 - e^{-K(t_p, 0) - F(t_p, 0)}}, \quad (41)$$

$$\sigma_0 = 4 \frac{\int_0^{t_p} dt' D_{\text{eff}}(t') e^{-2K(t_p, t')}}{1 - e^{-2K(t_p, 0)}} \quad (42)$$

secure the time-periodicity of the solution. Quasi-static conditions correspond to slow driving relative to the relaxation times $\tau_H = 1/(\mu k + D_r)$ and $\tau_\sigma = 1/(2\mu k)$ for H and σ , respectively. It allows the dynamics of the functions H and σ to be regarded as relaxed, $\dot{H} = \dot{\sigma} = 0$, from which one gets the quasi-static variance

$$\sigma(t) = \sigma_\infty(t) \equiv \frac{2}{k} \left(T + \frac{v^2}{2\mu} \frac{1}{k\mu + D_r} \right). \quad (43)$$

The leading correction in the driving speed is derived in App. B. Conversely, if the driving is fast relative to the relaxation times τ_H and τ_σ , the colloid cannot respond to the changing parameters k , T , v and D_r , and its variance is given by Eq. (43) with time-averaged parameter values.

At intermediate rates, the complete expression (40) has to be used. To make sure that we calculate the nested integral correctly, we cross-check the obtained results with two independent methods, BD simulations and numerical solutions [80]. The finite-time variances follow the quasi-static ones like carrot-chasing donkeys, i.e., the variance decreases (increases) if it is larger (smaller) than the stationary value σ_∞ corresponding to the given value of the control parameters, cf. Figs. 3 (b)-(d). The discrepancy between the quasi-static and the finite-time predictions increases for faster driving and moreover grows with the activity ratio $v_{>}/v_{<}$. As intuitively expected, and suggested by the role of v in Eq. (38), larger active velocities lead to larger variances.

D. Effective temperature

Comparing Eqs. (10), (13), and (38) we find for the effective temperature of the ABE on the limit cycle

$$T_{\text{eff}}(t) = \frac{D_{\text{eff}}(t)}{\mu} = T(t) + \frac{v(t)H(t)}{2\mu}. \quad (44)$$

Its value is always larger than the bath temperature T . Apart from the latter, it also depends on the activity v , mobility μ , trap stiffness k , and rotational diffusion coefficient D_r . All the parameters, except for T , enter T_{eff} indirectly, and in a complex way, through the differential equation (37) for H . The effective temperature thereupon acquires the characteristic relaxation time, $\tau_H = (\mu k + D_r)^{-1}$. Its quasi-static limiting form (14) explicitly reads

$$T_{\text{eff}}(t) \rightarrow T_{\text{eff}}^\infty(t) \equiv \frac{k\sigma_\infty}{2} = T + \frac{v^2}{2\mu} \frac{1}{k\mu + D_r}. \quad (45)$$

The effective temperature possesses several counter-intuitive features. First, in case of periodically modulated activity or trap stiffness, it varies in time, even if the bath temperature is held constant. Moreover, due to its dynamical nature and finite relaxation time, it generally does so even when both bath parameters T and v are held constant. Hence, to realize a proper (effectively) isothermal process with constant T_{eff} , one has to carefully tune the control parameters. This is most easily achieved under quasi-static conditions, as demonstrated in Fig. 2e). There we plot the effective temperature (44) (full blue line) and also its quasi-static limit (45), which would be obtained at very slow driving (black dotted line). For the chosen parameters, the quasi-static effective temperature (45) runs *approximately* along a Stirling cycle, in accord with the temperature $T(t)$ and activity $v(t)$ [Figs. 2 (b) – (d)]. Conversely, the finite-time effective temperature (44) exhibits substantially different behavior.

Before going into more details, we now outline three thermodynamically consistent interpretations of the ABE model and derive the corresponding entropy productions. In the discussion of quasi-static and finite-time performance of the engine in Secs. IX A and IX B, respectively, we utilize these entropy productions as examples of variables that are not captured by the effective-temperature mapping (19). Another example is the full distribution of the particle position, which we discuss in Appendix D.

VIII. ENTROPY PRODUCTION

As a genuinely non-equilibrium system, any active heat engine always produces entropy, even if operated infinitely slowly. However, how much of that entropy we can (or care to) track depends on our experimental resolution (and interpretation of the engine).

A. User perspective

On the coarsest level of description, which might be adopted by a *user* of the heat engine, only the supplied heat and the harvested output work matter. Their ratio is the natural measure of efficiency, which is bounded by the optimum (Carnot) efficiency determined by the effective temperature T_{eff} . As we have discussed, this temperature can experimentally be measured for the model of a trapped Brownian particle, namely by a device sensible to the variance σ of the particle position; see Fig. 4 a). The thermodynamics of the active heat engine is thereby mapped to that of an ordinary engine with an equilibrium bath and obeys the same limitations. Accordingly, the user would conclude that the total dissipated cycle entropy

$$\Delta S_{\text{tot}}^{\text{eff}} = \int_0^{t_p} dt \dot{S}_{\text{tot}}^{\text{eff}} = \int_0^{t_p} dt \dot{S}_{\text{R}}^{\text{eff}} \quad (46)$$

is given by the net entropy change per cycle in the bath, which thus solely controls the degree of irreversibility of the cycle. To compute the latter, the user would resort to the expression given in Eq. (22) of Sec. VI A, namely

$$\dot{S}_{\text{R}}^{\text{eff}} = -\dot{Q}/T_{\text{eff}} \equiv \dot{Q}_{\text{dis}}^{\text{eff}}/T_{\text{eff}}. \quad (47)$$

Since the particle dynamics is modelled within an overdamped Stokes approximation, the corresponding “effective” dissipation $Q_{\text{dis}}^{\text{eff}}$ to the effective equilibrium bath is straightforwardly given by the force acting on the particle times its velocity (averaged)

$$\dot{Q}_{\text{dis}}^{\text{eff}} = -\langle \nabla_{\mathbf{r}} V \cdot \dot{\mathbf{r}} \rangle = -k(t)\dot{\sigma}(t)/2. \quad (48)$$

Importantly, the user is not concerned with other details of the non-equilibrium bath than the variance σ and the effective equilibrium temperature T_{eff} it provides. He would thus adopt the above expressions for arbitrary noise in Eq. (2), regardless of the underlying physics of the bath. For the specific ABE realisation of the active heat engine, these expressions can explicitly be evaluated using Eqs. (38), (40) and (44).

B. Trajectory perspective

In contrast to the user, a *heat engineer* would possibly consider the engine at a higher resolution and have access to the individual stochastic *trajectories* of the particle position generated by Eq. (2). Thereby, she could uncover the non-equilibrium character of active heat bath that dissipates energy even if the engine operates under quasi-static conditions. To this end, she could evaluate the dissipation per cycle in the form $\langle \log P_{\text{F}}(\Gamma)/P_{\text{R}}(\Gamma^*) \rangle$, exploiting a relation often referred to as local detailed balance condition. It relates the symmetry breaking between the path probabilities $P_{\text{F}}(\Gamma)$ and $P_{\text{R}}(\Gamma^*)$ for paths Γ and their time-reversed images Γ^* to dissipation. (For more details, see App. C and Refs. [81, 82].) The method can in principle be applied regardless of the physics underlying the noise term in Eq. (2), if one can observe or otherwise guess the time-reversed dynamics. See Ref. [82] for an example of a successful application of such a strategy to biological systems. In general, this will however technically require assumptions or knowledge of the time-reversed noise dynamics, i.e., microscopic information beyond that of the stochastic (forward) trajectories of the particle position. Such information is seldom available outside the realm of detailed models of the mesoscopic physics. For specificity, we therefore now consider the above ABE based on the ABP model.

C. ABP perspective: sailboats versus surfboards

For ABP’s, the noise $\boldsymbol{\eta}$ comprises the (time-symmetric) equilibrium white noise $\sqrt{2D}\xi$ together with the active

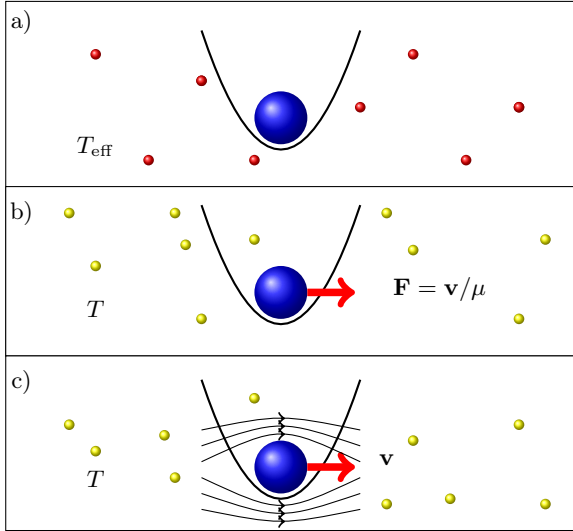


FIG. 4. Different levels of control over the system imply different changes in the bath entropy. a) Mere “users” of an active heat engine are only concerned with its thermodynamic input/output characteristics. They judge reversibility and entropy changes with respect to an effective equilibrium bath [red particles] at a fictitious temperature T_{eff} larger than the temperature T of the background solvent [yellow particles in b) and c)]. A more detailed knowledge of the engine’s internal working substance (the ABP particle) and its dynamics allows one to uncover the non-equilibrium character of the system, which depends on the time-reversal properties of its dynamics. If the active velocity \mathbf{v} in the ABE results from dragging or pushing the particle through the liquid by an external force \mathbf{F} [panel b)], the particle behaves like a sailboat and the change in bath entropy obeys Eq. (52). If the particle is advected by the surrounding liquid with velocity \mathbf{v} like a surfboard [panel c)], the entropy change in the bath obeys Eq. (53).

propulsion \mathbf{v} . The colloid could be a randomly (self-) propelled active particle or a schematically modelled passive tracer in an active bath [5, 29]. In any case, its active velocity \mathbf{v} is due to a dissipative process and admits two alternative interpretations, depending on its presumed time-reversal properties. Namely, it can be understood as a Stokes velocity caused by an external (random) force $\mathbf{v}(t)/\mu$, the so-called swim force. This very common interpretation, depicted in Fig. 4) b), treats the particle like a sailboat blown around by erratic winds, which is why we refer to it as the “sailboat” interpretation. Or, in a second interpretation, depicted in Fig. 4) c), the active term $\mathbf{v}(t)$ can be interpreted as the actual swim velocity of a microswimmer that either “sneaks” through the quiescent background solvent by an effective phoretic surface slip $\mathbf{v}(t)$ [83–85] or is passively advected by a local flow field $\mathbf{v}(t)$ [86]. We refer to it as the “surfboard” interpretation. It treats $\mathbf{v}(t)$ as a proper dynamic velocity as opposed to the disguised force in the sailboat interpretation. Upon time-reversal, forces usually do not change

the sign, while velocities do. The detailed balance condition then implies that the rate of entropy change in the bath reads

$$\dot{S}_{\text{R}}^{\pm} = \dot{Q}_{\text{dis}}^{\pm}/T, \quad (49)$$

for sailboats (+) and surfboats (−), respectively [87–89]. The dissipation rates are

$$\dot{Q}_{\text{dis}}^{+} = \langle (\mathbf{v}/\mu - \nabla_{\mathbf{r}}V) \cdot \dot{\mathbf{r}} \rangle = \dot{Q}_{\text{dis}}^{\text{eff}} + v^2/\mu - \langle \nabla_{\mathbf{r}}V \cdot \mathbf{v} \rangle, \quad (50)$$

$$\dot{Q}_{\text{dis}}^{-} = \langle -\nabla_{\mathbf{r}}V \cdot (\dot{\mathbf{r}} - \mathbf{v}) \rangle = \dot{Q}_{\text{dis}}^{\text{eff}} + \langle \nabla_{\mathbf{r}}V \cdot \mathbf{v} \rangle. \quad (51)$$

We refer to App. C for details of the formal derivation, and discuss these results on a physical basis. In the dissipation rate \dot{Q}_{dis}^{+} for sailboats, the swim term is added as an additional force (intuitively the wind drag) to the potential force. In contrast, for surfboards, it is subtracted from the particle velocity corresponding to a reformulation of the equation of motion in a frame that is freely co-moving with the flow velocity $\mathbf{v}(t)$.

Since $\dot{Q}_{\text{dis}}^{+}(t)$ and $\dot{Q}_{\text{dis}}^{-}(t)$ have different reference points (vanishing for sailboats blown against the quay and surfboards floating freely with the surf, respectively), the two dissipation rates can not generally be ordered according to their magnitude for the ABE, where both situations may (approximately) be encountered along the cycle. Also note that the detailed balance condition imposes that the heat is dissipated in the background solvent at temperature $T(t)$, which is natural from the point of view of the ABP model. As a consequence, also different amounts of entropy production will be assigned to the self-propulsion, dependent on the chosen ABP interpretation.

They can both be understood as composed of the effective dissipation $\dot{Q}_{\text{dis}}^{\text{eff}}(t)$ over the solvent temperature $T(t) \leq T_{\text{eff}}(t)$, plus some extra (manifestly active) entropy production due to the particle’s excursions off the surf or off the quay, respectively,

$$T\dot{S}_{\text{R}}^{+} = \dot{Q}_{\text{dis}}^{\text{eff}} + v^2/\mu - 2\mu k(T_{\text{eff}} - T), \quad (52)$$

$$T\dot{S}_{\text{R}}^{-} = \dot{Q}_{\text{dis}}^{\text{eff}} + 2\mu k(T_{\text{eff}} - T). \quad (53)$$

In the second case (surfboards), the additional propulsion contribution to the entropy production beyond $\dot{S}_{\text{R}}^{\text{eff}}$ is manifestly positive, since $T_{\text{eff}} \geq T$. Intuitively, this is because any failure to float with the flow gives rise to dissipation. In the first case (sailboats), the minimum condition for $\dot{S}_{\text{R}}^{\text{eff}}$ can only be guaranteed under quasi-static conditions. Intuitively, the “wind” may otherwise transiently prevent dissipation by “arresting the sailboat at the quay”.

While the derivation of the expressions (52) and (53) relies on a deeper knowledge of the system dynamics than the behavior of the variance, it is worth noting that $\sigma(t)$ is still sufficient for their evaluation. The dynamics of the variance thus suffices to evaluate the “total” entropy

$\Delta S_{\text{tot}}^{\pm}(t_p) = S_{\text{R}}^{\pm}(t_p) = \int_0^{t_p} dt \dot{S}_{\text{R}}^{\pm}$ produced per cycle of the operation of the ABE. In contrast, the change in the system entropy

$$S(t) = - \int_{-\infty}^{\infty} dx \int_{-\infty}^{\infty} dy \int_0^{2\pi} d\theta p \log p, \quad (54)$$

which vanishes for a complete cycle but is necessary for evaluating the total entropy change within the cycle, $\Delta S_{\text{tot}}^{\pm}(t) = S_{\text{R}}^{\pm}(t) + S(t) - S(0)$, depends on the full probability distribution $p(x, y, \theta, t)$ for the position of the particle at time t . The latter obeys the Fokker-Planck equation

$$\frac{\partial p}{\partial t} = \left(\nabla_{\mathbf{r}} \cdot [\mu \nabla_{\mathbf{r}} V(\mathbf{r}) - \mathbf{v}] + D \nabla_{\mathbf{r}}^2 + D_{\text{r}} \frac{\partial^2}{\partial \theta^2} \right) p \quad (55)$$

corresponding to Eqs. (35) and (36). One can calculate the PDF $p(x, y, \theta, t)$ either numerically, from Eq. (55), or using BD simulations of Eqs. (35)–(36) (see App. D for a detailed discussion of the results). The system entropy $S(t)$ is thus the only variable of our thermodynamic analysis which generally cannot be calculated using the mean square displacement σ alone.

The above results are suitable to fully quantify the engine’s thermodynamic performance. In the following section we evaluate the general expressions and discuss their generic properties.

IX. ABE-PERFORMANCE

In this section, we first focus on the quasi-static regime of operation of the ABE, where we demonstrate in more detail some peculiarities connected with the unintuitive behavior of the effective temperature. For vanishing entropy productions $\Delta S_{\text{tot}}^{\pm}$, as defined in the previous section, the non-equilibrium ABE bath is seen to admit a representation as an equilibrium bath. Then, we consider finite-time effects onto the performance of the ABE, and the additional entropy production due to the non-quasi-static operation.

A. Quasi-static regime

In the quasi-static regime, the engine dynamics in terms of the variance $\sigma(t)$ and the effective temperature $T_{\text{eff}}(t)$ are given by Eqs. (43) and (45), respectively. They thus depend merely parametrically on the driving $k(t)$, $T(t)$, $D_{\text{r}}(t)$, and $v(t)$. The effective entropy production $\Delta S_{\text{tot}}^{\text{eff}}$ (20) then vanishes, and the (effective) efficiency of the ABE is given by the classical result evaluated in terms of the stiffness $k(t)$ and temperature $T_{\text{eff}}(t)$. In particular, a quasi-static cycle consisting of two branches with constant T_{eff} and two adiabats will thus operate with Carnot efficiency η_{C} , (31). Equivalently, realizing a Stirling cycle in terms of $k(t)$ and the effective temperature $T_{\text{eff}}(t)$ will result in the (effective) Stirling efficiency

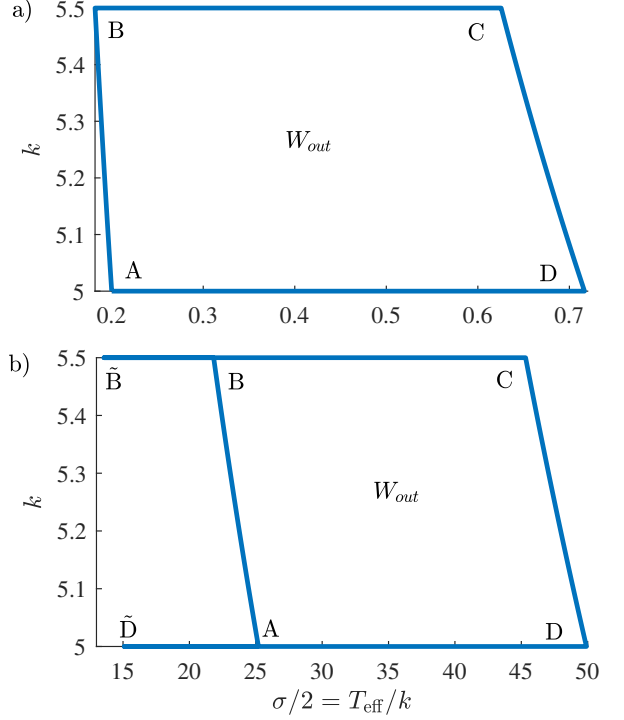


FIG. 5. Two quasi-static (generalized) Stirling cycles in terms of the trap stiffness $k(t)$ and variance $\sigma(t)$ of the particle positions ABCD and AB \tilde{B} CD \tilde{D} . (The corresponding energy flows are evaluated in Fig. 6.) a) In the standard Stirling cycle ABCD, the heat flows from the bath into the system along the isochor BC and isotherm CD ($\dot{Q} = k\dot{\sigma}/2 > 0$), and from the system into the bath otherwise ($\dot{Q} < 0$). b) In the “nonstandard Stirling” cycle AB \tilde{B} CD \tilde{D} , the heat flow reverses (outflow along B \tilde{B} , inflow along \tilde{B} C) along the isochoric branch BC = B \tilde{B} C and similarly for the isochor DA = D \tilde{D} A. The output works $W_{\text{out}} = 0.5 \int_0^{t_p} dk \sigma$ of the individual cycles are given by the areas they enclose. Similarly, heat input and output can be visualized as areas below the curves.

$\eta_{\text{C}} \log a / (\eta_{\text{C}} + \log a)$ with $a = \min(k) / \max(k)$ [29]. And one could deal similarly with other thermodynamic cyclic protocols. However, using the simplifying analogy with the effective equilibrium bath, one should make sure to actually use $k(t)$ and $T_{\text{eff}}(t)$ as control parameters and not simply rely on an intuition about the behavior of the effective temperature based on the background solvent temperature T , activity v and rotational diffusivity D_{r} . Indeed, as mentioned in Sec. VIID, what is a Stirling (or Carnot) cycle in terms of the effective temperature can be quite different from the one defined in terms of T , v , and D_{r} . To quantify the difference, it is useful to introduce the parameter

$$\mathcal{K}(t) \equiv k\mu / D_{\text{r}} \quad (56)$$

which compares the characteristic timescales D_{r}^{-1} and $(k\mu)^{-1}$ for relaxation of the orientation θ and the posi-

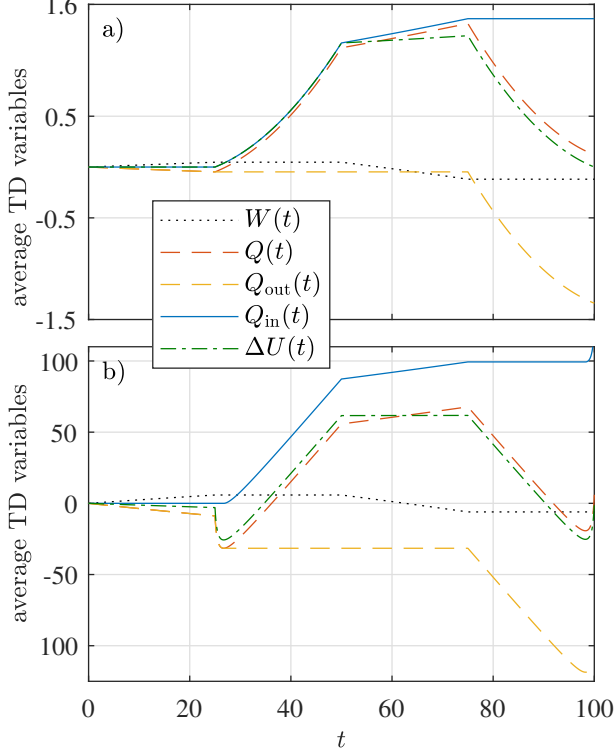


FIG. 6. Energy flows for the quasi-static Stirling cycles depicted in Fig. 5. Net work and heat W , $Q = |Q_{\text{in}}| - |Q_{\text{out}}|$, heat influx and outflux Q_{in} , Q_{out} and internal energy change $\Delta U = U(t) - U(0)$, as defined in Sec. IV are traced out as functions of time during a quasi-static cycle of duration $t_p = 100$ significantly larger than the relaxation times $\tau_H = 1/(\mu k + D_r)$ and $\tau_\sigma = 1/(2\mu k)$ for T_{eff} and σ , respectively. Panel a) $v_> = 4$. Panel b) $v_> = 500$, $v_< = 50$, $D_r^> = 500$ and $D_r^< = 5$; other parameters as in Fig. 2.

tion \mathbf{r} , respectively. The quasi-static effective temperature (45) can be written as

$$T_{\text{eff}}(t) = T + \frac{v^2}{2\mu D_r} \frac{1}{1 + \mathcal{K}}. \quad (57)$$

Only in the limiting cases $\mathcal{K} \rightarrow 0$ and $\mathcal{K} \rightarrow \infty$, a *naive* quasi-static isothermal process (constant temperature T , activity v , and D_r) corresponds to an effective equilibrium isothermal process (constant T_{eff}).

Despite the equilibrium analogy, the bath actually corresponds to a driven system with its apparent equilibrium characteristics actively maintained by some dissipative processes. So even for quasi-static operation of the engine, closer inspection reveals this non-equilibrium nature of the bath. In particular, the sailboat/surfboard interpretations of the particle motion will reveal some of this entropy production, so that $\Delta S_{\text{tot}}^\pm \geq \Delta S_{\text{tot}}^{\text{eff}}$.

For strong confinements, $\mathcal{K} \gg 1$, the active dynamics is highly persistent on the confinement scale, so that the

particle moves quasi-ballistically in the potential. The effective temperature T_{eff} is therefore given by the temperature of the equilibrium solvent T , which is the only remaining source of noise. Using the sailboat interpretation of the ABP (where \mathbf{v} is interpreted as an external force), we find that $\Delta S_{\text{tot}}^+ = \Delta S_{\text{tot}}^{\text{eff}} = 0$. The sailboat interpretation is thus consistent with the notion that the ABE operates reversibly, in this limit. In contrast, the surfboard (for which \mathbf{v} is interpreted as a velocity) dissipates, since its free motion clashes with the confinement by the potential, so that $\Delta S_{\text{tot}}^- = \Delta S_{\text{tot}}^{\text{eff}} + \int_0^{t_p} dt v^2(t)/\mu = \int_0^{t_p} dt v^2(t)/\mu > 0$.

For weak confinements, $\mathcal{K} \ll 1$, the particle's active motion randomizes on the confinement scale so that it can be subsumed into the δ -correlated noise (33) via the effective temperature and the corresponding noise correlation matrix $C_{ij}(t, t') = 2\sqrt{D_{\text{eff}}(t)D_{\text{eff}}(t')}\delta_{ij}\delta(t - t')$. Its dynamics mimics Brownian motion in an effective equilibrium bath maintained at the (stiffness-independent) temperature $T_{\text{eff}} = T + v^2/(2\mu D_r)$. In this case, confinement and random active motion interfere in such a way that both the sailboat and surfboard interpretations can detect the positive entropy production, $\Delta S_{\text{tot}}^\pm > \Delta S_{\text{tot}}^{\text{eff}} = 0$, and the actual irreversibility of the operation. Only by imposing the additional limit $v^2 \ll 2\mu D_r$, when the rotational motion completely obliterates the active swimming, surfboards cease to be bothered by the confinement and no longer dissipate, so that $\Delta S_{\text{tot}}^- = 0$. In the sailboat interpretation, this corresponds to a complete waste of the efforts of the external swim force, so that it still reflects the irreversibility via $\Delta S_{\text{tot}}^+ = \int_0^{t_p} dt v^2(t)/\mu > 0$.

For intermediate values of \mathcal{K} , the effective temperature depends on the stiffness $k(t)$ and the (traditional) definition of heat input along an individual step of the driving protocol may not actually yield the correct interpretation. It then also fails to yield a consistent measure of efficiency. Instead, one should carefully reconsider what is the actual heat input, based on Eq. (9), which can be rewritten as $Q_{\text{in}} = \frac{1}{2} \int_0^{t_p} dt' k \dot{\sigma} \Theta[\dot{\sigma}]$. Heat thus flows into the system whenever the variance σ — and thus the effective system entropy (26) — increases, and vice versa.

To illustrate this point, recall the definition of the Stirling cycle in Sec. VII B. The standard Stirling cycle consists of two isochores (constant trap stiffness k) and two isotherms (constant solvent temperature T). Therefore it forms a rectangle in a k - T diagram, translating to a shape similar to the ABCD cycle in Fig. 5, in a k - T/k diagram. Actually, Fig. 5 is slightly more general, as it shows two possible interpretations of the quasi-static ABE-Stirling cycle in a k - T_{eff}/k diagram. The “standard” protocol ABCD corresponds to the evolution of the thermodynamic variables as depicted in Fig. 6a). Note that they, in turn, evolve strictly monotonically or remain constant during the individual steps of duration $t_p/4$. Hence, during a single step, heat is either only absorbed or only released by the system, and it is possible to write the input heat as $Q_{\text{in}} = Q_{\text{BC}} + Q_{\text{CD}}$, where Q_{XY} is the amount

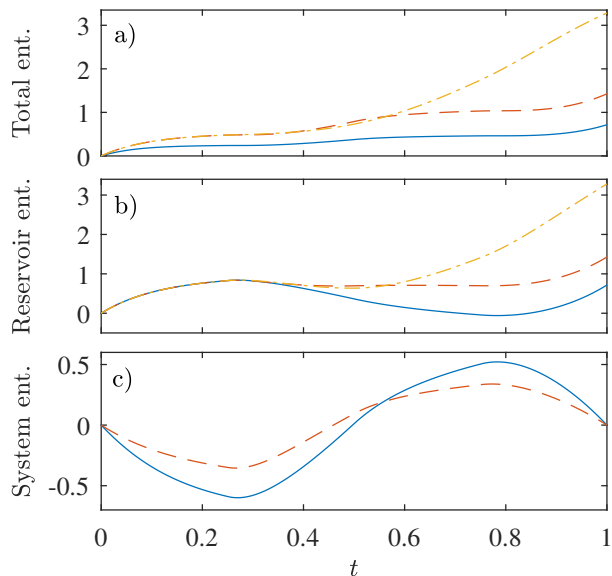


FIG. 7. Evolution of the various entropies discussed in the text as functions of time during the limit cycle, depicted in Fig. 2, with $v_> = 4$. Panel a) “total” ABE entropy changes ΔS_{tot}^+ for “sailboats”, (red dashed line), $\Delta S_{\text{tot}}^-(t)$ for “surfboards” (yellow dot-dashed line), both from Sec. VIII C, and the effective entropy change $\Delta S_{\text{tot}}^{\text{eff}}(t)$ from Eq. (29) (solid blue line). Panel b) shows corresponding changes in the reservoir entropy $\Delta S_{\text{R}}^+(t)$ from Eq. (52) (red dashed line), $\Delta S_{\text{R}}^-(t)$ from Eq. (53) (yellow dot-dashed line), and $\Delta S_{\text{R}}^{\text{eff}}(t)$ from integrating Eq. (22) (solid blue line), and panel c) in the system entropy $\Delta S^{\text{eff}}(t)$ from Eq. (58) (solid blue line) and $\Delta S(t)$ from Eq. (59) (red dashed line).

of heat absorbed between the points X and Y . Which corresponds to the conventional practice for a Stirling cycle.

Consider next the cycle $AB\tilde{B}C\tilde{D}\tilde{D}$ corresponding to Fig. 6b). In this case, the system releases heat during the segment $B\tilde{B}$ (σ decreases from σ_B to $\sigma_{\tilde{B}}$), but absorbs heat during the remainder of the state change BC (σ increases from $\sigma_{\tilde{B}}$ to σ_C). A similar situation occurs also at the end of the cycle. Hence, the conventional shorthand notion of heat input as heat exchanged between the system and the reservoir during an entire step of the cycle is not appropriate, in this case. Instead, one has to use the definition (9), also utilized in Fig. 6. The dashed red, dashed yellow and full blue lines in Fig. 6b) in the time interval from $t = 25$ to $t = 50$, also serve to illustrate the differences in the heat balance. For a further treatment of efficiency of Stirling engines operating in contact with active baths in the quasi-static regime, we refer to Ref. [29].

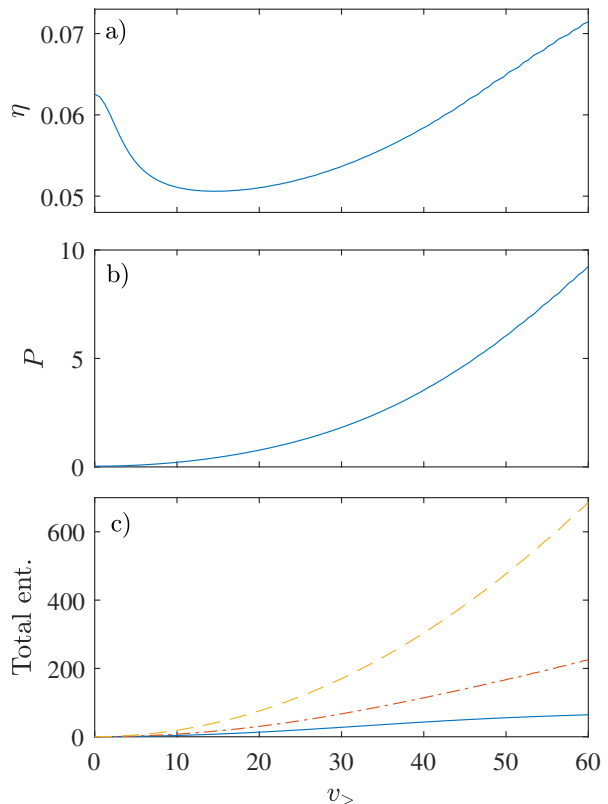


FIG. 8. Efficiency a), power output b), both from Eq. (8), and total entropy production c), as functions of the maximum active velocity $v_>$ for the protocol from Fig. 2. Panel c) ΔS_{tot}^- (yellow dashed), ΔS_{tot}^+ (red dot-dashed), and $\Delta S_{\text{tot}}^{\text{eff}}$ (solid blue), all from Eq. (60).

B. Finite-time performance

Let us finally investigate the most complex case of non-quasi-static cycles for which the protocol from Sec. VII B is imposed with cycle durations t_p significantly shorter than the internal relaxation times $\tau_H = 1/(\mu k + D_r)$ and $\tau_\sigma = 1/(2\mu k)$ for T_{eff} and σ , respectively. The ABE model provides full control over the finite-time thermodynamics. To check our analytical results for the variance given in Sec. VII C, we compared it to direct numerical solutions of the equations of motion via the matrix numerical method of Ref. [80], and found perfect agreement. We also note that the new features observed in the analytical results for the toy model are generic, and should qualitatively also be observed for other heat engines in contact with non-equilibrium reservoirs.

The hallmark of non-quasi-static operation of any thermodynamic heat engine is the observation of a net entropy increase during the cycle. Therefore, Fig. 7 depicts the individual entropy changes defined in Secs. VI A and VIII as functions of time during the limit cycle. Panel

a) shows that both the total effective entropy change $\Delta S_{\text{tot}}^{\text{eff}}(t)$, measured by the ABE user, and the total ABE entropy changes $\Delta S_{\text{tot}}^{\pm}(t)$, corresponding to the sailboat and surfboard interpretations, are non-decreasing functions of time. They thus meet the expectation for valid total entropies according to the second law of thermodynamics. It is noteworthy, that the ABE entropy changes $\Delta S_{\text{tot}}^{\pm}(t)$ are larger than the effective entropy change $\Delta S_{\text{tot}}^{\text{eff}}(t)$, at all times, even during the first part of the cycle, given by $t \in (0, 0.25)$, where the active velocity v vanishes.

As gleaned from the panel b), the rates of entropy change in the bath, with $\dot{S}_{\text{R}}^{\text{eff}}$ given by Eq. (22) and $\dot{S}_{\text{R}}^{\pm}(t)$ given by Eqs. (52) and (53), are in that case all equal. The inequality $\Delta S_{\text{tot}}^{\text{eff}}(t) < \Delta S_{\text{tot}}^{\pm}(t)$ is then solely caused by the different changes of the system entropy

$$\Delta S^{\text{eff}}(t) = S^{\text{eff}}(t) - S^{\text{eff}}(0) = \log \frac{\sigma(t)}{\sigma(0)}, \quad (58)$$

$$\Delta S(t) = S(t) - S(0), \quad (59)$$

shown in the panel c), with $S^{\text{eff}}(t)$ and $S(t)$ given by Eqs. (26) and (54), respectively. For the remaining time [$t \in (0.25, 1)$] of the cycle, even the changes in the bath entropies $\Delta S_{\text{R}}^{\pm}(t)$ of the ABE are larger than $\Delta S_{\text{R}}^{\text{eff}}(t)$. While $\dot{S}_{\text{R}}^-(t) \geq \dot{S}_{\text{R}}^{\text{eff}}(t)$ and $\dot{S}_{\text{tot}}^{\pm} \geq \dot{S}_{\text{tot}}^{\text{eff}}$ always hold, we find that $\dot{S}_{\text{R}}^+(t) < \dot{S}_{\text{R}}^{\text{eff}}(t)$ is not ruled out (detailed data now shown). The figure also corroborates the periodicity of the system entropies $S^{\text{eff}}(t)$ and $S(t)$, so that the total entropy changes $\Delta S_{\text{tot}}^{\text{eff}}(t_p)$ and $\Delta S_{\text{tot}}^{\pm}(t_p)$ per cycle are solely determined by the (per cycle) entropy changes $\Delta S_{\text{R}}^{\text{eff}}(t_p)$ and $\Delta S_{\text{R}}^{\pm}(t_p)$ in the bath, as it should be.

To study the influence of activity on the ABE performance, in Fig. 8, we fix $t_p \equiv 1$ for various maximum active velocities $v_{>}$ according to Fig. 2. For small values of $v_{>}$ the efficiency is decreased by the activity, while for large values of $v_{>}$ it is increased, and eventually attains a constant maximum value. This behavior can be understood as follows. The efficiency of the heat engine quite generally increases with the largest difference in the effective temperature $\max(T_{\text{eff}}) - \min(T_{\text{eff}})$, similarly as in the Carnot formula. Even beyond the quasi-static regime one expects that the effective temperature is qualitatively described by Eq. (45). For small values of $v_{>}$, Eq. (45) implies that the temperature difference can be decreased by variations of the rotational diffusion coefficient, depicted in Fig. 2c), while it increases with $v_{>}$ for large $v_{>}$. More intuitive behavior is observed for the power Fig. 8b) and the entropy productions $\Delta S_{\text{tot}}^{\text{eff}}$ and $\Delta S_{\text{tot}}^{\pm}$ Fig. 8c) that monotonically increase with $v_{>}$.

Finally, we assess the effect of the finite-time driving on the ABE operation. Specifically, in Fig. 9, we depict performance of the ABE as function of the cycle duration t_p for three values of the maximum active velocity $v_{>}$. In panel a), the efficiency monotonously increases with increasing t_p and eventually reaches the quasi-static limit (the red line). Notably, whether the efficiency is increased or decreased by the bath activity depends on the cycle duration, as evidenced by the

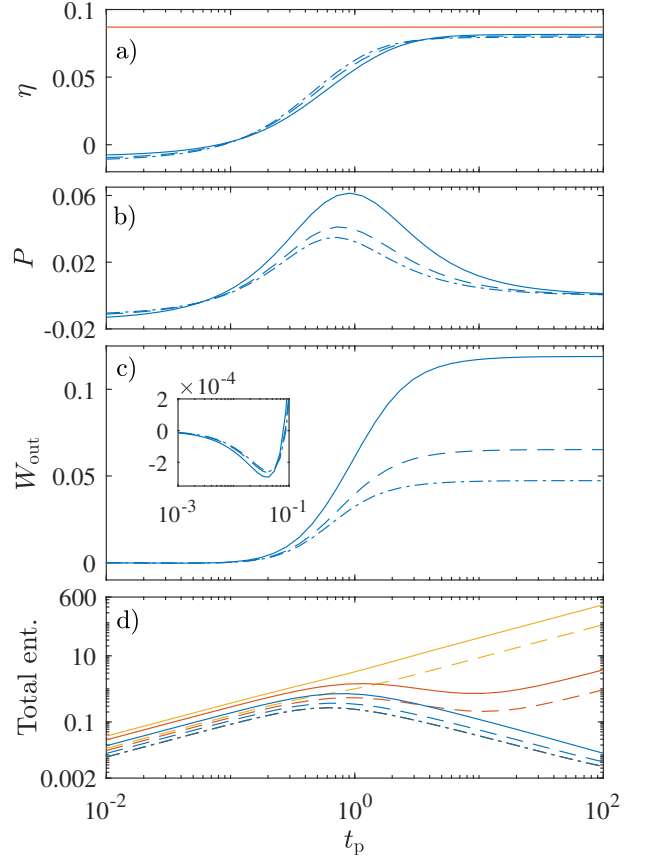


FIG. 9. Efficiency a), output power b), and output work c), defined in Sec. IV, and total entropy production d) for $v_{>} = 0$ (dot-dashed lines), $v_{>} = 2$ (dashed lines) and $v_{>} = 4$ (full lines) as functions of cycle duration t_p . The inset in panel c) magnifies the initial part of the plot for $t_p \in [10^{-3}, 10^{-1}]$. Panel d) $\Delta S_{\text{tot}}^{\text{eff}}$ (yellow), ΔS_{tot}^+ (red), and ΔS_{tot}^- (blue); all according to Eq. (60). Other parameters as in Fig. 2.

dashed and dot-dashed lines wandering above and below the solid line. Namely, apart from enhancing the output work and power [panels b) and c)], the activity also provides an increased heat flow into the system. As expected, the output power vanishes for large cycle durations and exhibits a maximum for a certain value of t_p . On the contrary, the output work is, for large cycle times, an increasing function which converges to the quasi-static value, which monotonously increases with $v_{>}$. Interestingly, for $10^{-2} \lesssim t_p \lesssim 10^{-1}$, the output work exhibits a shallow negative excursion as revealed by the blowup in the inset. This implies a lower bound $t_p \approx 10^{-1}$ on the cycle duration, below which the system ceases to operate as a heat engine.

As can be observed in Fig. 9d), for small and large cycle durations, the cycle-time dependence of the total entropy productions $\Delta S_{\text{tot}}^{\text{eff}}(t_p)$ and $\Delta S_{\text{tot}}^{\pm}(t_p)$ exhibits asymptotic power-law behavior. Taylor expansions of the total entropy productions in t_p and $1/t_p$, respectively, give $\Delta S_{\text{tot}}^{\pm} \propto \Delta S_{\text{tot}}^{\text{eff}} \propto t_p$ for short t_p and $\Delta S_{\text{tot}}^{\pm} \propto t_p^{-1}$ for large t_p .

for $v \neq 0$, and $\Delta S_{\text{tot}}^{\text{eff}} \propto 1/t_p$ regardless of v , for long t_p . To be more specific, all the total entropy productions in question assume the form

$$\Delta S_{\text{tot}}^x = - \int_0^{t_p} dt \frac{1}{\mathcal{T}(t)} \left(\dot{Q} + \mathcal{F} \right) (t), \quad (60)$$

where $\mathcal{T} = T_{\text{eff}}$ and $\mathcal{F} = 0$ for $x = \text{eff}$, $\mathcal{T} = T$ and $\mathcal{F} = -2\mu k(T_{\text{eff}} - T)$ for $x = -$, and $\mathcal{T} = T$ and $\mathcal{F} = 2\mu k(T_{\text{eff}} - T) - v^2/\mu$ for $x = +$. For fast driving of the engine, (t_p much smaller than the intrinsic relaxation times), the colloid cannot react to the changing driving and settles on a time-independent state corresponding to a mean value of the driving. Hence, Eq. (60) can be approximated for all x by $\Delta S_{\text{tot}}^x \approx -t_p \left(\dot{Q} + \mathcal{F} \right) / \mathcal{T}$, where the integrand is evaluated using the time-independent state attained for $t_p \rightarrow 0$.

For slow driving (t_p much smaller than the intrinsic relaxation times), the colloid attains its steady state (43) independently of the cycle duration t_p . Substituting the integration time t in Eq. (60) by the dimensionless time $\tau = t/t_p$ yields

$$\Delta S_{\text{tot}}^x = -t_p \int_0^1 d\tau \frac{1}{\tilde{\mathcal{T}}(\tau)} \left(\frac{1}{t_p} \frac{d\tilde{Q}(\tau)}{d\tau} + \tilde{\mathcal{F}}(\tau) \right), \quad (61)$$

where $\tilde{\mathcal{T}}(\tau) = \mathcal{T}(\tau t_p)$, $\tilde{Q}(\tau) = Q(\tau t_p)$, and $\tilde{\mathcal{F}}(\tau) = \mathcal{F}(\tau t_p)$. The effective total entropy production $\Delta S_{\text{tot}}^{\text{eff}}$ vanishes in the limit $t_p \rightarrow \infty$, and thus the leading contribution in Eq. (61) is expected to be of order $1/t_p$. Indeed, expanding under the integral, we obtain (for $\mathcal{F} = 0$)

$$\frac{1}{\tilde{\mathcal{T}}} \frac{d\tilde{Q}}{d\tau} \approx \frac{d}{d\tau} \log \sigma_\infty + \frac{1}{t_p} C. \quad (62)$$

Since the first term represents a total derivative, the corresponding loop integral vanishes and what remains is the correction C/t_p . For $x = \pm$, the leading contribution to the integral (61) is simply determined by the non-zero value of $\lim_{t_p \rightarrow \infty} \mathcal{F}$ and thus we find $\Delta S_{\text{tot}}^\pm \propto t_p$ for large t_p . For $v = 0$, all three definitions of entropy production are equivalent since then $\mathcal{T} = T = T_{\text{eff}}$ and $\mathcal{F} = 0$. This proves the scalings found in Fig. 9d).

X. CONCLUSION AND OUTLOOK

We have derived a simple strategy to map the average thermodynamics of a linear Langevin system with arbitrary additive noise to an effective equilibrium model. The mapping is based on the matching of the dynamical equations for the second moment of position, which happens to determine the (average) energetics. It is valid for arbitrary protocols imposed by the time-dependent model parameters. In the quasi-static limit, the (generally time-dependent) effective temperature $T_{\text{eff}}(t)$ (4) that accomplishes the mapping recovers the known expression (14). A benefit of this mapping is that conventional bounds on the (both finite-time and quasi-static)

thermodynamic performance of machines, especially heat engines, carry over to those with non-equilibrium (active) baths [5, 29–31]. As a part of our discussion, we have therefore been able to provide a new perspective on recent claims of surprisingly high Stirling efficiencies (essentially corresponding to infinite temperature steps) in a bacterial heat engine that was experimentally realized by Krishnamurthy et al. [5].

We have exemplified these somewhat abstract notions for a specific model of a Brownian particle confined in a harmonic potential with periodically varying parameters. We call it the ABE, since the particle dynamics is based on the well-known active Brownian particle (ABP) model. Our qualitative conclusions should carry over to other designs, though. In particular, we find that the explicitly computed effective temperature T_{eff} has some non-intuitive features. (i) During the limit cycle, which is attained by the ABE at long times, it obeys a first-order differential equation and thus acquires some time dependence $T_{\text{eff}}(t)$ with a technically relevant characteristic relaxation time. (ii) It is important to realize that it can therefore vary in time even during those parts of the cycle in which the model parameters are held constant. (iii) Even in the quasi-static limit, T_{eff} depends on the strength of the potential. This means that realizing specific thermodynamic conditions, like an ‘‘isothermal’’ process with respect to the effective temperature, is generally not trivial.

The ABE model is also instructive with respect to some limitations of the effective-bath mapping. Namely, by construction, the latter is blind to the potentially rich features of the non-equilibrium bath beyond the second moment of the particle position, which we identified as the working degree of freedom of the engine. The effective description thus misses the non-Gaussian shape of the positional probability density and the corresponding Shannon entropy, for example, and also all housekeeping heat fluxes required to maintain the bath activity. Accordingly, we could demonstrate that the entropy production in the effective model can be understood as a lower bound for all conceivable practical and theoretical realizations. Namely, it vanishes upon quasi-static operation, whereas any detailed model of the bath dynamics would, like the explicitly studied ABE, necessarily reveal some of the housekeeping heat fluxes and their associated entropy production.

As an outlook, we would like to note that our analysis suggests some straightforward generalizations to arbitrary mobility and correlation matrices, thus also including under-damped dynamics. Furthermore, it should also be possible to generalize it to arbitrary linear memory kernels. Another possible extension could be the application of the presented method to non-linear systems, e.g., by deriving approximate time-dependent effective temperatures via suitable closures of the equations describing the relevant degrees of freedom.

ACKNOWLEDGMENTS

We acknowledge funding by Deutsche Forschungsgemeinschaft (DFG) via SPP 1726/1 and KR 3381/6-1, and

by Czech Science Foundation (project No. 20-02955J). VH gratefully acknowledges support by the Humboldt foundation. S.S. acknowledges funding by International Max Planck Research Schools (IMPRS).

-
- [1] S. Sánchez, L. Soler, and J. Katuri, *Angew. Chem. Int. Ed.* **54**, 1414 (2015).
- [2] P. Hänggi and F. Marchesoni, *Rev. Mod. Phys.* **81**, 387 (2009).
- [3] G. A. Ozin, I. Manners, S. Fournier-Bidoz, and A. Arsenault, *Adv. Mater.* **17**, 3011 (2005).
- [4] J. R. Baylis, J. H. Yeon, M. H. Thomson, A. Kazerooni, X. Wang, A. E. St. John, E. B. Lim, D. Chien, A. Lee, J. Q. Zhang, J. M. Piret, L. S. Machan, T. F. Burke, N. J. White, and C. J. Kastrup, *Sci. Adv.* **1** (2015).
- [5] S. Krishnamurthy, S. Ghosh, D. Chatterji, R. Ganapathy, and A. K. Sood, *Nat Phys* **12** (2016).
- [6] U. Seifert, *Phys. Rev. Lett.* **95**, 040602 (2005).
- [7] M. Esposito, U. Harbola, and S. Mukamel, *Rev. Mod. Phys.* **81**, 1665 (2009).
- [8] K. Sekimoto, *Stochastic Energetics*, Lecture Notes in Physics, Vol. 799 (Springer, 2010).
- [9] U. Seifert, *Rep. Prog. Phys.* **75**, 126001 (2012).
- [10] O. Abah, J. Roßnagel, G. Jacob, S. Deffner, F. Schmidt-Kaler, K. Singer, and E. Lutz, *Phys. Rev. Lett.* **109**, 203006 (2012).
- [11] J. Roßnagel, S. T. Dawkins, K. N. Tolazzi, O. Abah, E. Lutz, F. Schmidt-Kaler, and K. Singer, *Science* **352**, 325 (2016).
- [12] J.-P. Brantut, C. Grenier, J. Meineke, D. Stadler, S. Krinner, C. Kollath, T. Esslinger, and A. Georges, *Science* **342**, 713 (2013).
- [13] V. Blickle and C. Bechinger, *Nat Phys* **8** (2011).
- [14] I. Martinez, É. Roldán, L. Dinis, D. Petrov, J. Parrondo, and R. R.A., *Nat. Phys.* **12**, 67 (2015).
- [15] I. A. Martinez, E. Roldan, L. Dinis, and R. A. Rica, *Soft Matter* **13**, 22 (2017).
- [16] M. Esposito, R. Kawai, K. Lindenberg, and C. Van den Broeck, *Phys. Rev. E* **81**, 041106 (2010).
- [17] G. Verley, M. Esposito, T. Willaert, and C. Van den Broeck, *Nat. Commun.* **5** (2014).
- [18] K. E. Dorfman, D. V. Voronine, S. Mukamel, and M. O. Scully, *Proc. Natl. Acad. Sci. U.S.A.* **110**, 2746 (2013).
- [19] V. Holubec and A. Ryabov, *Phys. Rev. E* **96**, 030102(R) (2017).
- [20] M. Campisi and R. Fazio, *Nat. comm.* **7**, 11895 (2016).
- [21] P. Chvosta, M. Einax, V. Holubec, A. Ryabov, and P. Maass, *J. Stat. Mech: Theory Exp.* **2010**, P03002 (2010).
- [22] R. Kosloff and Y. Rezek, *Entropy* **19**, 136 (2017).
- [23] R. S. Whitney, *Phys. Rev. Lett.* **112**, 130601 (2014).
- [24] T. Schmiedl and U. Seifert, *EPL* **81**, 20003 (2008).
- [25] V. Holubec, *J. Stat. Mech: Theory Exp.* **2014**, P05022 (2014).
- [26] J. M. Horowitz and J. M. Parrondo, *Nat. Phys.* **8**, 108 (2012).
- [27] J. Roßnagel, O. Abah, F. Schmidt-Kaler, K. Singer, and E. Lutz, *Phys. Rev. Lett.* **112**, 030602 (2014).
- [28] W. Niedenzu, V. Mukherjee, A. Ghosh, A. G. Kofman, and G. Kurizki, *Nat. Commun.* **9**, 165 (2018).
- [29] R. Zakine, A. Solon, T. Gingrich, and F. van Wijland, *Entropy* **19**, 193 (2017).
- [30] D. Martin, C. Nardini, M. E. Cates, and É. Fodor, *EPL* **121**, 60005 (2018).
- [31] A. Kumari, P. Pal, A. Saha, and S. Lahiri, arXiv preprint arXiv:1912.00585 (2019).
- [32] G. Gompper, C. Bechinger, S. Herminghaus, R. Isele-Holder, U. B. Kaupp, H. Löwen, H. Stark, and R. G. Winkler, *Eur. Phys. J. Spec. Top.* **225**, 2061 (2016).
- [33] M. Cates, *Rep. Prog. Phys.* **75**, 042601 (2012).
- [34] Y. Fily and M. C. Marchetti, *Phys. Rev. Lett.* **108**, 235702 (2012).
- [35] G. Szamel, *Phys. Rev. E* **90**, 012111 (2014).
- [36] X.-L. Wu and A. Libchaber, *Phys. Rev. Lett.* **84**, 3017 (2000).
- [37] X. Zhao, K. K. Dey, S. Jeganathan, P. J. Butler, U. M. CĂşrdova-Figueroa, and A. Sen, *Nano Letters* **17**, 4807 (2017), pMID: 28726415.
- [38] L. Angelani, C. Maggi, M. L. Bernardini, A. Rizzo, and R. Di Leonardo, *Phys. Rev. Lett.* **107**, 138302 (2011).
- [39] J. Harder, S. A. Mallory, C. Tung, C. Valeriani, and A. Cacciuto, *J. Chem. Phys.* **141** (2014).
- [40] T. F. F. Farage, P. Krinninger, and J. M. Brader, *Phys. Rev. E* **91**, 042310 (2015).
- [41] W. T. Coffey, Y. P. Kalmykov, and J. T. Waldron, *The Langevin equation* (World Scientific, 2004).
- [42] D. Geiss, K. Kroy, and V. Holubec, *New J. Phys.* **21**, 093014 (2019).
- [43] D. Geiss, K. Kroy, and V. Holubec, *New J. Phys.* **21**, 119503 (2019).
- [44] V. Blickle and C. Bechinger, *Nat. Phys.* **8**, 143 (2012).
- [45] V. Holubec and A. Ryabov, *Phys. Rev. E* **96**, 062107 (2017).
- [46] V. Holubec and A. Ryabov, *Phys. Rev. Lett.* **121**, 120601 (2018).
- [47] Here and in the rest of the paper, we use the Stratonovich convention. See Sec. VIID for an explicit calculation of the effective temperature for the ABE model.
- [48] H. Callen, H. Callen, N. F. R. C. of Australia. Research Division, and W. . Sons, *Thermodynamics and an Introduction to Thermostatistics* (Wiley, 1985).
- [49] V. Holubec and A. Ryabov, *J. Stat. Mech.: Theory Exp.* **2016**, 073204 (2016).
- [50] T. Speck, *EPL* **114**, 30006 (2016).
- [51] R. Kubo, *Rep Progr. Phys.* **29**, 255 (1966).
- [52] C. Jarzynski, *Phys. Rev. Lett.* **78**, 2690 (1997).
- [53] G. E. Crooks, *Phys. Rev. E* **60**, 2721 (1999) (1999).
- [54] T. Hatano and S. I. Sasa, *Phys. Rev. Lett.* **86**, 3463ãÅŞ (2001).
- [55] T. R. Gingrich, J. M. Horowitz, N. Perunov, and J. L. England, *Phys. Rev. Lett.* **116**, 120601 (2016).
- [56] K. Proesmans and C. V. den Broeck, *EPL* **119**, 20001 (2017).
- [57] P. Pietzonka and U. Seifert, *Phys. Rev. Lett.* **120**,

- 190602 (2018).
- [58] G. Falasco, M. Esposito, and J.-C. Delvenne, arXiv preprint arXiv:1906.11360 (2019).
- [59] G. Falasco, M. V. Gnann, D. Rings, and K. Kroy, Phys. Rev. E **90**, 032131 (2014).
- [60] G. Falasco, M. V. Gnann, and K. Kroy, arXiv preprint arXiv:1406.2116 (2014).
- [61] R. Wulfert, M. Oechsle, T. Speck, and U. Seifert, Phys. Rev. E **95**, 050103(R) (2017).
- [62] U. M. B. Marconi, A. Puglisi, and C. Maggi, Sci. Rep. **7**, 46496 (2017).
- [63] J. Casas-Vazquez and D. Jou, Rep. Prog. Phys. **66**, 1937 (2003).
- [64] L. F. Cugliandolo, J. Phys. A: Math. Gen **44**, 483001 (2011).
- [65] D. GeiÅ§ and K. Kroy, ChemSystemsChem **1**, e1900041 (2019).
- [66] A way to overcome this limitation, leading to an approximate effective temperature, might be based on finding a suitable (approximate) closure for Eq. (18), so that it would only depend on a finite number of moments.
- [67] J. S. Lee and H. Park, Sci. Rep. **7**, 10725 (2017).
- [68] H. B. Callen, *Thermodynamics and an Introduction to Thermostatistics*, Student Edition (Wiley India Pvt. Ltd, 2006).
- [69] M. Esposito, R. Kawai, K. Lindenberg, and C. Van den Broeck, Phys. Rev. Lett. **105**, 150603 (2010).
- [70] V. Holubec and A. Ryabov, Phys. Rev. E **92**, 052125 (2015).
- [71] Y.-H. Ma, D. Xu, H. Dong, and C.-P. Sun, Phys. Rev. E **98**, 042112 (2018).
- [72] A. Ryabov, V. Holubec, M. H. Yaghoubi, M. Varga, M. E. Foulaadvand, and P. Chvosta, J. Stat. Mech: Theory Exp. **2016**, 093202 (2016).
- [73] M. Polettini, G. Verley, and M. Esposito, Phys. Rev. Lett. **114**, 050601 (2015).
- [74] C. Maes, J. Stat. Phys. **154**, 705 (2014).
- [75] C. Maes and S. Steffenoni, Phys. Rev. E **91**, 022128 (2015).
- [76] R. Zwanzig, J. Stat. Phys. **9**, 215 (1973).
- [77] S. Steffenoni, K. Kroy, and G. Falasco, Phys. Rev. E **94**, 062139 (2016).
- [78] U. M. B. Marconi, C. Maggi, and S. Melchionna, Soft Matter **12**, 5727 (2016).
- [79] X. Zheng, B. ten Hagen, A. Kaiser, M. Wu, H. Cui, Z. Silber-Li, and H. Löwen, Phys. Rev. E **88**, 032304 (2013).
- [80] V. Holubec, K. Kroy, and S. Steffenoni, Phys. Rev. E **99**, 032117 (2019).
- [81] C. Maes and K. Netočný, J. Stat. Phys. **110**, 269 (2003).
- [82] C. Battle, C. P. Broedersz, N. Fakhri, V. F. Geyer, J. Howard, C. F. Schmidt, and F. C. MacKintosh, Science **352**, 604 (2016).
- [83] B. Qian, D. Montiel, A. Bregulla, F. Cichos, and H. Yang, Chem. Sci. **4**, 1420 (2013).
- [84] K. Kroy, D. Chakraborty, and F. Cichos, Eur. Phys. J. Spec. Top. **225**, 2207 (2016).
- [85] U. Khadka, V. Holubec, H. Yang, and F. Cichos, Nat. Commun. **9**, 3864 (2018).
- [86] T. Speck, J. Mehl, and U. Seifert, Phys. Rev. Lett. **100**, 178302 (2008).
- [87] D. Chaudhuri, Phys. Rev. E **94**, 032603 (2016).
- [88] P. Pietzonka and U. Seifert, J. Phys. A **51**, 01LT01 (2018).
- [89] S. Shankar and M. C. Marchetti, Phys. Rev. E **98**, 020604(R) (2018).
- [90] N. Bleistein and R. A. Handelsman, *Asymptotic expansions of integrals* (Courier Corporation, 1975).
- [91] G. Nemes, *Asymptotic Expansions for Integrals*, Master's thesis, Loránd Eötvös University (2012).
- [92] D. Luposchinsky and H. Hinrichsen, J. Stat. Phys. **153**, 828 (2013).
- [93] H. Kleinert and H. Kleinart, *Path integrals in quantum mechanics, statistics, and polymer physics*, Vol. 400 (World Scientific, 1995).
- [94] H. Risken, *The Fokker-Planck Equation* (Springer, 1996) pp. 63–95.
- [95] Y. Fily, A. Baskaran, and M. F. Hagan, Soft Matter **10**, 5609 (2014).
- [96] H. H. Wensink and H. Löwen, Phys. Rev. E **78**, 031409 (2008).
- [97] R. Nosrati, P. J. Graham, Q. Liu, and D. Sinton, Sci. Rep. **6**, 26669 (2016).
- [98] J. Shin, A. G. Cherstvy, W. K. Kim, and V. Zaburdaev, Phys. Chem. Chem. Phys. **19**, 18338 (2017).
- [99] J. A. McLennan, Phys. Rev. **115**, 1405 (1959).
- [100] T. S. Komatsu and N. Nakagawa, Phys. Rev. Lett. **100**, 030601 (2008).
- [101] C. Maes and K. Netočný, J. Math. Phys. **51**, 015219 (2010).
- [102] D. A. Sivak and G. E. Crooks, Phys. Rev. Lett. **108**, 150601 (2012).
- [103] N. Nakagawa and S.-i. Sasa, Phys. Rev. E **87**, 022109 (2013).

Appendix A: Analytical solution for variance

Inserting the time correlation matrix (34) for the ABP model into Eq. (12), Eq. (10) yields the following dynamic equation for the variance $\sigma = \langle x^2 \rangle + \langle y^2 \rangle$:

$$\dot{\sigma} + 2\mu k \sigma = 4 \langle x_0 \eta_x(t) + y_0 \eta_y(t) \rangle e^{-K(t,t_0)} + 4D(t) + 2v(t) \int_{t_0}^t dt' v(t') e^{-K(t,t') - F(t,t')}, \quad (\text{A1})$$

where

$$K(t, t_0) = \mu \int_{t_0}^t dt' k(t'), \quad (\text{A2})$$

$$F(t, t_0) = \int_{t_0}^t dt' D_r(t'). \quad (\text{A3})$$

In order to explicitly evaluate the thermodynamics of the particular realization of an active Brownian heat engine described in Sec. VII, namely the ABP-based engine that we refer to as the ABE model, we need the solution of Eq. (A1). More precisely, we can concentrate onto the time periodic solution, which is attained by the system at late times, after transients have relaxed, so that it settles onto a limit cycle (c.f. Fig. 3). Taking the limit $t_0 \rightarrow -\infty$ in the formal solution to Eq. (A1), we obtain

$$\sigma(t) = 2 \lim_{t_0 \rightarrow -\infty} \int_{t_0}^t dt' [2D(t') + v(t')H(t')] e^{-2K(t,t')} \quad (\text{A4})$$

with

$$H(t) = \lim_{t_0 \rightarrow -\infty} \int_{t_0}^t dt' v(t') e^{-K(t,t') - F(t,t')}. \quad (\text{A5})$$

For the numerical evaluation of Eq. (A4) it is useful to exploit that $H(t)$ is a t_p -periodic function and to rewrite $K(t, t_0)$ as $K(t, t_0) = \lfloor (t-t_0)/t_p \rfloor K(t_p, 0) + K(t, t_0 + \lfloor (t-t_0)/t_p \rfloor t_p)$ using the t_p -periodicity of $k(t)$ (the symbol $\lfloor x \rfloor$ denotes the floor operation) and similarly for $F(t, t_0)$. Interestingly, using a simple trick, the time-periodic late-time limit can be found without considering the (numerically inconvenient) limit $t_0 \rightarrow -\infty$, just as in the case of memoryless dynamics [24, 25]. The key insight is that not only the function σ , but also H fulfills a certain differential equation, which can be obtained by taking the time derivative of Eq. (A5). The resulting formulas and the time-periodic solutions for σ and H are given in the main text in Sec. VII C.

Appendix B: Slow driving limit of variance

For slowly varying driving functions $k(t)$, $D(t)$, $D_r(t)$ and $v(t)$, the variance (A4) can be approximated using a simple formula which follows from the Laplace type approximation of the integral [90, 91]

$$\int_{t_0}^t dt f(t') e^{\int_{t'}^t dt'' g(t'')} = \int_{t_0}^t dt f(t') e^{t_p \int_{t'/t_p}^{t/t_p} dt'' g(t_p t'')} = \frac{f(t)}{g(t)} - \frac{1}{g^2(t)} \left[\dot{v}(t) - v(t) \frac{\dot{g}(t)}{g(t)} \right] + o(\dot{f}, \dot{g}). \quad (\text{B1})$$

Applying this approximation first on the function $H(t)$ (A5) and then on the variance $\sigma(t)$ (A4), we obtain the approximate result

$$\sigma(t) = \sigma_\infty - \frac{v^2}{k\mu\kappa^2} \left(\frac{\dot{v}}{v} - \frac{\dot{\kappa}}{\kappa} \right) - \frac{D}{k^2\mu^2} \left(\frac{\dot{D}}{D} - \frac{\dot{k}}{k} \right) - \frac{v^2}{2k^2\mu^2\kappa} \left(2\frac{\dot{v}}{v} - \frac{\dot{\kappa}}{\kappa} - \frac{\dot{k}}{k} \right) + o(\dot{v}, \dot{D}, \dot{k}, \dot{\kappa}). \quad (\text{B2})$$

Here, σ_∞ is the variance (43) for infinitely slow driving and $\kappa = \kappa(t) = k\mu + D_r$. For discontinuous driving, the limiting solution σ_∞ is also discontinuous. The first order correction (B2) may also be discontinuous if the first derivatives of the driving functions exhibit jumps. In such a case, however, the assumption on the smallness of the derivatives used in the calculation leading to Eq. (B2) is not valid. In accord with the discussion below Eq. (D1) in Appendix D, Eq. (B2) reveals that activity-corrections are at least second order in v .

Appendix C: Entropy production from path probabilities

The entropy

$$\Delta S_{R,\Gamma}(t) = \log(P_F/P_R) \quad (\text{C1})$$

delivered to the bath by a particle moving along a trajectory $\Gamma(t) = \{\mathbf{r}(t'), \theta(t')\}_{t'=0}^t$ of the stochastic process (35), (36) is given by the logarithm of the ratio of conditional probabilities P_F and P_R [81, 92], for the trajectory conditioned with respect to its initial point and its time-reversed image. Up to normalization, the forward probability is given by

$$P_F \propto e^{-2 \int_0^t dt' [\boldsymbol{\xi} \cdot \boldsymbol{\xi} + \xi_\theta^2]}, \quad (\text{C2})$$

where the noise terms $\boldsymbol{\xi} = [\dot{\mathbf{r}} + \mu \nabla_{\mathbf{r}} V - \mathbf{v}]/\sqrt{2D}$ and $\xi_\theta = \dot{\theta}/\sqrt{2D_r}$ follow from Eqs. (35) and (36) [93]. The backward probability is given by a similar formula. One just has to change the sign before quantities which are odd with respect to time reversal.

Assuming the active velocity $\mathbf{v} = v(\cos \theta, \sin \theta)$ to be time-reversal even, the odd variables in Eqs. (35) and (36) are time derivatives, giving

$$(P_F/P_R)^+ = e^{-\int_0^t dt' (\nabla_{\mathbf{r}} V - \mathbf{v}/\mu) \cdot \dot{\mathbf{r}}/T}, \quad (\text{C3})$$

whereas, for time-reversal odd \mathbf{v} , we find

$$(P_F/P_R)^- = e^{-\int_0^t dt' \nabla_{\mathbf{r}} V \cdot (\dot{\mathbf{r}} - \mathbf{v})/T}. \quad (\text{C4})$$

The entropy delivered to the reservoir during time interval $(0, t)$ follows as

$$\Delta S_{R,\Gamma}(t) = \langle \Delta S_{R,\Gamma}(t) \rangle_\Gamma = \langle \log(P_F/P_R) \rangle_\Gamma, \quad (\text{C5})$$

where the average is taken over the individual realizations Γ of the stochastic process [92]. With Eq. (C3) for the time-even active velocity, it yields

$$\Delta S_{R^+}(t) = \int_0^t dt' \frac{1}{T} \left\langle \left(\frac{\mathbf{v}}{\mu} - \nabla_{\mathbf{r}} V \right) \cdot \dot{\mathbf{r}} \right\rangle, \quad (\text{C6})$$

and with Eq. (C4), for the time-odd active velocity,

$$\Delta S_{R^-}(t) = \int_0^t dt' \frac{1}{T} \langle (\dot{\mathbf{r}} - \mathbf{v}) \cdot (-\nabla_{\mathbf{r}} V) \rangle. \quad (\text{C7})$$

Appendix D: Probability distributions (PDFs)

In the 3-dimensional Langevin system (35)–(36), the $x - y$ coordinates are coupled via the active velocity \mathbf{v} . The steady probability distribution (PDF) to find the particle with orientation θ at position (x, y) thus cannot generally be written in the separated form $p(x, y, \theta) = \chi(x, \theta)\iota(y, \theta) = \chi(x, \theta)\chi(y, \pi/2 - \theta)$, where $\chi(x, \theta)$ solves the 2-dimensional Fokker–Planck equation

$$\partial_t \chi = [D \partial_x^2 + D_r \partial_\theta^2 + \partial_x (\mu \partial_x V - v \cos \theta)] \chi. \quad (\text{D1})$$

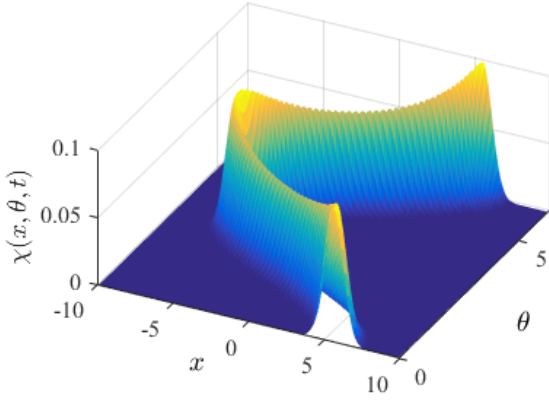


FIG. 10. Probability distribution χ for particle position x and orientation θ at the end of the hot isotherm ($t = 3t_p/4$, see Fig. 2). We take $v_{>} = 30$ and $t_p = 10^4$. Other parameters are the same as in Fig. 2.

Inserting the separation ansatz into the 3-dimensional equation (55) and using the formula (D1) leads to the condition $2D_r \partial_\theta \chi(x, \theta) \partial_\theta \iota(y, \theta) = 0$ that cannot be fulfilled in general. Nevertheless, one can still reduce the 3-dimensional system to just two degrees of freedom by introducing the polar coordinates $x = r \cos \phi$, $y = r \sin \phi$. Then, Eq. (35) transforms to

$$\dot{r} = -kr + v \cos(\theta - \phi) + \sqrt{2D} \eta_r, \quad (\text{D2})$$

$$\dot{\phi} = \frac{v}{r} \sin(\theta - \phi) + \sqrt{\frac{2D_r}{r^2}} \eta_\phi, \quad (\text{D3})$$

while θ still obeys Eq. (36). The symbols η_r and η_ϕ denote independent, zero-mean, Gaussian white noises. Since Eqs. (D2) and (D3) only depend on the difference $\theta - \phi$, introducing the relative angle $\psi = \theta - \phi$, subject to the zero-mean, Gaussian white noise η_ψ renders them in the form

$$\dot{r} = -kr + v \cos \psi + \sqrt{2D} \eta_r, \quad (\text{D4})$$

$$\dot{\psi} = -\frac{v}{r} \sin \psi + \sqrt{2 \left(\frac{D_r}{r^2} + D \right)} \eta_\psi. \quad (\text{D5})$$

The corresponding Fokker–Planck equation for the PDF $\rho = \rho(r, \psi, t)$ reads [94]

$$\partial_t \rho = \left[D \partial_r^2 + \left(\frac{D_r}{r} + D \right) \partial_\psi^2 \right] \rho - \cos \psi \partial_r (v \rho) - D \partial_r \left(\frac{\rho}{r} \right) + k \partial_r (r \rho) + \frac{v}{r} \partial_\psi (\sin \psi \rho). \quad (\text{D6})$$

In general, the equations (D1) and (D6) [or, equivalently (55)] can not be solved analytically and thus we solved them using the numerical method described in Ref. [80]. We compared the numerical solution of Eq. (D6) to the separated ansatz $p(x, y, \theta) = \chi(x, \theta) \chi(y, \pi/2 - \theta)$ and found out that, although not exact, the ansatz describes

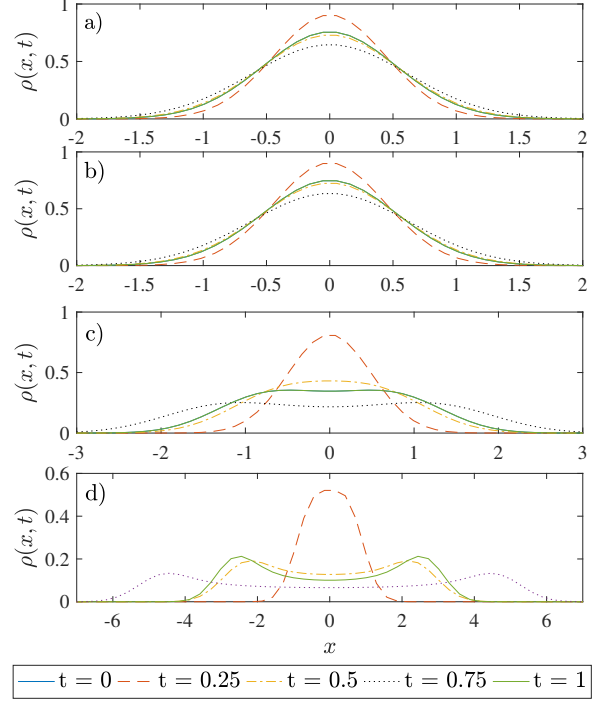


FIG. 11. Marginal distribution ρ for the particle position x at the end of the individual branches of the cycle for different values of the maximum active velocity a) $v_{>} = 0$, b) $v_{>} = 1$, c) $v_{>} = 10$, and d) $v_{>} = 30$. We have set $t_p = 1$, corresponding to non-stationary driving, other parameters as in Fig. 2. Note that the curves at $t = 0$ and $t = 1$ are equal, in accord with the time periodic operation.

the full 3-dimensional PDF $p(x, y, \theta)$ sufficiently well. Since the 2-dimensional PDF allows for a more intuitive discussion and exhibits the main qualitative features of $p(x, y, \theta)$, we restrict the following discussion to $\chi(x, \theta)$.

Figure 10 shows a snapshot of the PDF $\chi(x, \theta, t)$, solution of (D1), at the end of the third branch of a quasi-static cycle introduced in Sec. VII B (the hot “isotherm”). The figure reveals the typical shape of the PDF χ , with two global maxima located at $\theta = 0$ and π , which survives even for rapid driving protocols. Physically, the shape of the PDF can be understood as follows: 1) for any fixed orientation angle θ , the PDF can be expected to exhibit a maximum at the position where the active velocity (which acts in the Langevin Eq. (35) for x as a force $v \cos \theta / \mu$) is balanced by the force kx exerted by the parabolic potential; 2) the projection $v \cos \theta / \mu$ of \mathbf{v} on the x -coordinate changes slowest around its extrema (0 and π), and thus most trajectories contribute to the surroundings of these points, making the extrema for 0 and π largest.

Figure 11 shows snapshots of the marginal PDF $\rho(x, t) = \int d\theta \chi(x, \theta, t)$ for the position x at the beginning of the individual branches of the cycle, for four values of

the maximum active velocity $v_{>}$. With increasing $v_{>}$, the resulting PDFs become increasingly non-Gaussian and finally even exhibit two separated peaks. Physically, this behavior can be understood by the wall accumulation effect due to the persistence of the active motion [95–97], which creates the double peak during the cycle branches with large $v_{>}$. (For similar PDFs, see Ref. [79, 98].) Qualitatively similar results are also obtained in the quasi-static limit, as already apparent from Fig. 10.

To get some intuition about these results on analytical grounds, we now present several approximate solutions to Eq. (D1). Different from the standard diffusion ($v = 0$) in an external potential, the quasi-static ($\partial_t \chi = 0$) solution of the Fokker-Planck equation (D1) is not given by the Boltzmann PDF. This is because one cannot subsume the activity into a generalized potential \tilde{V} which would act as a Lyapunov functional for the dynamics of x and θ . Nevertheless, there are several limiting cases where the Boltzmann form $\chi \propto \exp(-\tilde{V}/T)$ is still a useful approximation.

The best analytical insight into the described qualitative properties of the presented numerical solutions to Eq. (D1) with time-dependent parameters is obtained for rotational diffusion coefficient D_r much smaller than $k\mu$, corresponding to the limit of large \mathcal{K} in Eq. (56). Then, the direction of the active velocity can be treated as quenched, so that the activity can be subsumed into a generalized potential $\tilde{V} = kx^2/2 - vx \cos \theta/\mu$. The corresponding quasi-static solution of Eq. (D1) then reads

$$\chi = \frac{1}{Z_\chi} \exp\left(\frac{vx \cos \theta}{\mu T} - \frac{kx^2}{2T}\right), \quad (\text{D7})$$

with a normalization constant Z_χ . For each fixed value of the angle θ , the PDF is then Gaussian with its maximum value $\exp[v^2 \cos^2 \theta / (2T\mu^2 k)] / Z_\chi$ at the position $v \cos \theta / (\mu k)$. The PDF thus possesses two global maxima located at $(x, \theta) = [v/(\mu k), 0]$ and $(x, \theta) = [-v/(\mu k), \pi]$, and is qualitatively similar to the PDF shown in Fig. 10.

The marginal PDF for x obtained from (D7) then reads

$$\rho(x, t) = \int d\theta \chi = \frac{1}{Z_\rho} \exp\left(-\frac{kx^2}{2T}\right) I_0\left(\frac{vx}{\mu T}\right). \quad (\text{D8})$$

Here, $I_0(x)$ denotes the modified Bessel function of the first kind and Z_ρ is another normalization constant. The marginal PDF is Gaussian for $v = 0$, and becomes more and more non-Gaussian with increasing $v/(\mu k)$. For large values of $v/(\mu k)$, it can even become bimodal. This behavior can be traced back to the shift of the maxima of the PDF χ with increasing $v/(\mu k)$. For small $v/(\mu k)$, the two maxima substantially overlap and the integration over the angle θ yields a single peak which is nearly Gaussian. For large values of $v/(\mu k)$, the two peaks do not overlap any more and the marginal PDF thus also exhibits two peaks. The behavior of the marginal PDF obtained in the limit $D_r \ll \mu k$ thus shows qualitatively the same behavior as the solution of Eq. (D1) shown in Fig. 11.

For D_r much larger than $k\mu$, corresponding to the limit of small \mathcal{K} in Eq. (56), the quasi-static PDF is given by $\chi \propto \exp(-V/T_{\text{eff}})$. This is because the rotational diffusion obliterates any persistence of the active motion, and the non-equilibrium bath effectively behaves like an equilibrium one with the renormalized temperature $T_{\text{eff}} = T + v^2/(2\mu D_r)$. In this limit, the degrees of freedom x and y also become independent.

Yet another case admitting an analytical solution of Eq. (D1), is that of quasi-static driving at small active velocity. Then the quasi-static PDF ρ can be approximated by the McLennan-type form $\chi \approx \exp(-U/T)[1 - W(x)]$ [99–103]. Without going into details, the function $W(x)$ is in general proportional to the (average) dissipation in the driven system [101], which, in our case, is given by the product of the active “force” $\mu^{-1}v \cos \theta$ and the particle velocity \dot{x} . Since the average over the angle θ of the active force is zero, the correction $W(x)$ to the particle PDF is seen to be at least second order in v .